PREVALENT POLYMORPHISM IN THYROID HORMONE-ACTIVATING ENZYME LEAVES A GENETIC FINGERPRINT THAT UNDERLIES ASSOCIATED CLINICAL SYNDROMES

[1]Elizabeth A. McAninch*, [1]Sungro Jo*, [1]Nailliw Z. Preite, [2,3]Erzsébet Farkas, [2,4]Petra Mohácsik, [2,5]Csaba Fekete, [2,4]Péter Egri, [2]Balázs Gereben, [6]Yan Li, [6]Youping Deng, [7]Mary Elizabeth Patti, [8]Chantal Zevenbergen, [8]Robin P. Peeters, [9]Deborah C. Mash, [1]Antonio C. Bianco,

*Both authors contributed equally to this manuscript.

[1]Division of Endocrinology and Metabolism, Rush University Medical Center, Chicago, IL 60612, USA;
[2]Department of Endocrine Neurobiology, Institute of Experimental Medicine, Hungarian Academy of Sciences, Budapest, H-1083, Hungary;
[3]Péter Pázmány Catholic University, Multidisciplinary Doctoral School of Sciences and Technology, Budapest, H-1083 Hungary
[4]Semmelweis University, János Szentágothai PhD School of Neurosciences, Budapest, H-1085 Hungary;
[5]Division of Endocrinology, Diabetes and Metabolism, Tufts Medical Center, Boston, MA 02111, USA;
[6]Department of Medicine, Rush University Medical Center, Chicago, IL 60612, USA
[7]Joslin Diabetes Center, Harvard Medical School, Boston, MA 02215, USA;
[8]Division of Endocrinology, Rotterdam Thyroid Center, Department of Internal Medicine, Erasmus MC, Rotterdam, The Netherlands;
[9]Department of Neurology, University of Miami Miller School of Medicine, Miami, FL 33136, USA

Abbreviated Title: THR92ALA D2 GENETIC FINGERPRINT

Key terms: Deiodinase, Polymorphism, Thr92AlaD2, Hypothyroidism, Transcriptome, Microarray

Word Count: 6055

Corresponding author and person to whom reprint requests should be addressed:

Antonio C. Bianco, M.D, Ph.D.
Division of Endocrinology and Metabolism
Rush University Medical Center
1735 W Harrison St; 212 Cohn Building; Chicago, IL 60612
Email: abianco@deiodinase.org
Phone: 312-942-7131
Fax: 312-942-5271

Disclosure Statement: The authors have nothing to disclose

Abstract

Context: A common polymorphism in the gene encoding the activating deiodinase (Thr92Ala-D2) is known to be associated with quality of life in millions of patients with hypothyroidism and with several organ-specific conditions. This polymorphism results in a single amino acid change within the D2 molecule where its susceptibility to ubiquitination and proteasomal degradation is regulated.

Objective: To define the molecular mechanisms underlying associated conditions in carriers of the Thr92Ala-D2 polymorphism.

Design, Setting, Patients: Microarray analyses of nineteen postmortem human cerebral cortex samples were performed to establish a foundation for molecular studies via a cell model of HEK-293 cells stably expressing Thr92 or Ala92 D2.

Results: The cerebral cortex of Thr92Ala-D2 carriers exhibits a transcriptional fingerprint that includes sets of genes involved in CNS diseases, ubiquitin, mitochondrial dysfunction (chromosomal genes encoding mitochondrial proteins), inflammation, apoptosis, DNA repair and growth factor signaling. Similar findings were made in Ala92-D2-expressing HEK-293 cells and in both cases there was no evidence that thyroid hormone signaling was affected, i.e. the expression level of T3-responsive genes was unchanged, but that several other genes were differentially regulated. The combined microarray analyses (brain/cells) led to the development of an 81-gene classifier that correctly predicts the genotype of homozygous brain samples. In contrast to Thr92-D2, Ala92-D2 exhibits longer half-life and was consistently found in the Golgi. A number of Golgi-related genes were down-regulated in Ala92-D2-expressing cells but were normalized after 24h-treatment with the antioxidant N-acetylecysteine.

Conclusions: Ala92-D2 accumulates in the Golgi, where its presence and/or ensuing oxidative stress disrupts basic cellular functions and increases pre-apoptosis. These findings are reminiscent to disease mechanisms observed in other neurodegenerative disorders such as Huntington's disease, and could contribute to the unresolved neurocognitive symptoms of affected carriers.

Introduction

Hypothyroidism is found in about 4.6 percent of the U.S. population age 12 and older (1). The current standard of care for these patients is treatment with daily tablets of the long-lived pro-thyroid hormone (TH), levothyroxine (L-T4). T4 is subsequently activated to T3 outside of the thyroid parenchyma via the deiodinases, i.e. D1 and D2. Unfortunately therapy with L-T4 alone does not resolve symptoms in all hypothyroid patients, with approximately 12% of the patients remaining symptomatic despite normalization of serum TSH and TH levels (2, 3). Impaired cognition, fatigue and difficulty losing weight are the main residual symptoms of these patients, for which we lack understanding and have no mechanistic explanation.

A prevalent Thr92Ala-D2 polymorphism (between 12-36% of the population are homozygotes (4)) has been identified that results in a single amino change at position 92 within an 18 amino acid loop that controls D2 ubiquitination for proteasomal destruction (5, 6). Hypothyroid individuals carrying this polymorphism were found to have a preference for a therapy that includes T3 vs. monotherapy with L-T4 alone (7), suggesting defective Ala92-D2 catalysis. In addition, the Thr92AlaD2 polymorphism has been associated with conditions aside from symptomatic hypothyroidism such as mental retardation (8), low IQ (9) and bipolar disorder (10); this supports the hypothesis that Ala92-D2-expressing is disruptive aside from impaired T4 activation.

Here we used a multifaceted strategy to define the molecular foundation of the clinical syndromes associated with the Thr92AlaD2 polymorphism. There are unique modifications in the cellular transcriptome identified in human brains homozygous for the polymorphism that are independent of TH signaling. These transcriptional changes included upregulation of processes related to the mitochondria, Golgi apparatus/ER transport, oxidative stress and apoptosis, suggesting a molecular basis underlying cerebral symptomatology in affected individuals. A cellular model revealed that Ala92-D2 protein exhibits a longer

half-life and, as opposed to Thr92-D2, can be found in the Golgi apparatus. Cells expressing Ala92-D2 also exhibited alteration in expression of Golgi markers, a finding that absolved with antioxidant treatment. Notably, in both the human brain and cell models there is molecular and physiological evidence of dysregulation in EGF receptor signaling, a pathway known to be altered in oxidative stress (11) and play an important role in cognitive development (12) and function (13-16).

Materials and Methods

Human Brain Samples

The University of Miami (UM) Brain Endowment Bank provided genomic DNA and brain tissue samples from postmortem human donors; protocols at UM were IRB-approved. Cause of death was limited to accident or sudden cardiac death without medical intervention or prolonged agonal state. Postmortem interval at specimen collection was <24 hours, brain pH (quality measure) was >6.0. Genomic DNA from 95 brain samples was genotyped for the Thr92AlaD2 polymorphism by sequence analysis according to previously published methods (17). Brain samples from 19 patients without known thyroid or neurologic disease (six from homozygous Thr92-D2, seven heterozygotes and six homozygotes for Ala92-D2) were matched by age (ANOVA $p = 0.46$), sex (male), race (Caucasian) and BMI (ANOVA $p = 0.66$) and chosen for further studies. Homogenous samples were dissected from frozen coronal blocks based on surface and cytoarchitectural landmarks from Brodmann's Area 38 (temporal cortex) by neuroanatomist and stored at -80°C.

Microarray Studies of Human Brain

RNA was extracted (RNeasy Lipid Tissue Mini Kit, Qiagen) and cDNA generated (First Strand cDNA Synthesis Kit, Roche). RNA from all 19 human brain samples from each of the three genotypes (Ala92-

D2 homozygotes, Hets, and Thr92-D2 homozygotes) was analyzed by microarray at the Joslin Diabetes Center Genomics Core Laboratory (Boston, MA). Gene expression was evaluated using Genechip Human Gene 2.0 ST arrays (Affymetrix, Santa Clara, CA) which utilizes a whole-transcript design to assess >30,000 coding genes. Gene expression data was preprocessed using Affymetrix Expression Console. Differential expression analysis was performed in Affymetrix Transcriptome Analysis Console to identify individual genes demonstrating enrichment in three comparisons: Ala92-D2 homozygotes vs. Thr92-D2 homozygotes (Table S2), Ala92-D2 homozygotes vs. Hets and Hets vs. Thr92-D2 homozygotes. Expression values (signal) of individual genes were $\log_2$ transformed. One-way ANOVA was used to calculate *p*-values for each fold change (linear); multi-testing correction was then performed using the Benjamini-Hochberg Step-Up FDR-controlling procedure for all the expressed genes. Genes were considered statistically significant with an ANOVA *p*-value <0.05. A custom heat map displaying expression values of the 25 with the highest and lowest fold change was generated (HeatMapViewer, GenePattern, Broad Institute).

Gene ontology analysis was used to determine differences in gene sets between phenotypes (Gene Set Enrichment Analysis (GSEA), Broad Institute). Expression values for all genes from all 19 brain samples were used; no filter was applied to eliminate genes with low expression. GSEA included calculation of enrichment scores (ES), estimation of significance level of ES (nominal *p*-value), and adjustment for multiple hypothesis testing including the normalized enrichment score (NES) and false discovery rate (FDR). Gene sets with an FDR ≤25% were limited (3) and given the goal of hypothesis generation, a nominal p-value of <1% was chosen to indicate significance. Core enrichment of individual genes within these gene sets was defined as those genes contributing to the leading-edge subset. All individual genes demonstrating core enrichment within the enriched gene sets were further considered by investigators (investigator analysis); this consisted of searches in publically available databases (PubMed, UniProt). A heatmap of the top 50 ranking genes from each genotype was generated by GSEA. GSEA was also applied to an investigator-generated custom gene set of known T3-responsive genes (18, 19).

Pathway analysis was performed with Ingenuity Pathway Analysis (IPA). The signal intensity values from the entire microarray dataset (all genes, all 19 samples) were used to identify canonical pathways altered between the three genotypes. When viewing the EGF Signaling pathway alone ($p < 0.001$, ratio 50/56 genes), individual genes demonstrating alteration in our dataset were highlighted in an IPA-generated pathway diagram.

Class prediction was performed (WeightedVoting, GenePattern) via two approaches. First the algorithm created a 10-gene classifier that was able to correctly predicted the genotypes of 12/12 samples; 2 of these 10 genes were SNORD16 and TRAPPC4. Then, the weighted voting prediction algorithm was used with an investigator-derived list of 79 genes as a classifier, where 11/12 sample genotypes were correctly predicted. Lastly, the 79-gene classifier was supplemented with the addition of SNORD16 and TRAPPC4 and applied to the microarray data from the Thr92-D2 and Ala92-D2 homozygotes.

Generation of stable cell lines and cell culture

HEK-293 cells (American Type Culture Collection, Manassas, VA) were cultured in 150-mm dishes with DMEM (Life Technologies) supplemented with 10% fetal bovine serum (FBS). Unless noted otherwise, all experiments were performed with 10% FBS-containing media. In particular, HEK-293 cells were chosen for this experiment as they express low levels of the deiodinases (20) and TR (21) and because they have certain properties consistent with neuronal lineage (22, 23).

The 6×His-CysD2-YFP (D2) vector was created fusing enhanced yellow fluorescent protein (EYFP) in frame to the C terminus of 133Cys/266Cys (CysD2) mutant human D2. The D2-EYFP cassette was inserted in-frame between *Eco*RI-*Not*I of pcDNA™4/ HisMax C (Invitrogen). The Thr92Ala (T92A) mutant of 133Cys/266Cys was generated by overlap extension PCR. HEK-293 cell lines stably expressing

wild type Thr92-D2^{HY} or polymorphic Ala92-D2^{HY} were established by transfecting 2.5 μg of His-D2-YFP vector using Lipofectamine 2000 reagent (Invitrogen) according to manufacturer's instructions. D2^{HY}-expressing clones of HEK-293 cells were selected 48h after transfection by antibiotic resistance (Zeocin, 300 μg/mL) for 2 weeks. The control yellow fluorescent protein (YFP)-expressing vector has been described elsewhere (24); these D2^{HY}-expressing cells exhibit similar properties compared to cells with native D2 (24). Some cells were grown to confluence and then treated with 1mM N-acetylecysteine (NAC, Sigma) or 1M trimethylamine-N-oxide (TMAO, Sigma) for 24 hours. In addition, some cells were treated with brefeldin A (BFA, Tocris), dissolved in abs ethanol for 30 minutes at 0.5ug/mL and then processed for electron microscopy (EM).

Flow Cytometry

BD FACSCalibur flow cytometer was used for these studies. For apoptosis, Annexin V-PE apoptosis detection kit (eBioscience) was used for annexin V cell surface staining per manufacturer's protocol. For cell cycle analysis, cells were collected, washed and resuspended. -20°C absolute ethanol was added in dropwise manner to the cell while vortexing. HEK-293 cells were fixed for 1h at 4°C. After washing twice, 40 g/ml propidium iodide and 1 g/ml RNase were added and incubated 3h at 4°C and subsequently analyzed by FACS. All of the FACS data were obtained after correct compensation setting using single labeled control. For cell size analysis, forward scatter was used as a measure of relative size.

Co-culture of Thr92-D2^{HY} and Ala92-D2^{HY}-expressing cells with T3-responsive HeLa cells

As a positive control, HeLa cells were grown to confluence in solutions of 0nM T3 or 100nM T3 (19) and harvested for RT-qPCR of known T3-responsive genes, BCL3 and SPOT14; both genes were significantly increased in the 100nM confirming T3-responsiveness in our system. Then, Thr92-D2^{HY} and Ala92-D2^{HY} HEK cells were grown to confluence in the upper chamber of a Transwell permeable support

(Corning) above, but not in physical contact with, highly T3-responsive HeLa cells (American Type Culture Collection) in 10% FBS. HeLa cells were harvested, RNA extracted and processed for RT-qPCR of T3-responsive genes.

Immunofluorescence

Cells were plated on poly-D-lysine-coated chamber slides and fixation, imaging and colocalization were performed as previously described (25). D2 was imaged with 1:500 αYFP (Rockland immunologicals) and 1:1000 α–nuclear lamin (Cell Signaling). For the Golgi immunofluorescence, cells were grown on culture slide until confluent. After fixation in 4% paraformaldehyde (Electron Microscopy Science) for 30 min, cells were permeabilized by 0.5% Triton X-100 and subsequently blocked by Fish Skin Gelatin (Biotum). GM130 antibody (CellSignaling technology) and antiGFP antibody (Rockland immunologicals) were added at 1ug/ml concentration at 4C overnight. Secondary antibodies (Life Technologies) were incubated for an hour and made into slide using SloFade Gold mounting medium (Life Technologies). Images were acquired using Nikon eclipse Ti microscope with C1 confocal system. Images were subsequently analyzed by NISelement AR or ImageJ software

For immunofluorescence after CHX treatment, each chamber was fixed as previously described (26) and then incubated in a mixture of mouse Na^+/K^+ATPase antiserum (Santa Cruz, (M7-PB-E9) at 1:250 dilution and rabbit GFP antiserum at 1:10000 dilution in PBS containing 2% normal horse serum and 0.2% sodium azide (antiserum diluent) for 2 days at 4°C. After rinses in PBS, the cells were incubated in biotinylated donkey anti-mouse IgG for 2h (1:500; Jackson Immunoresearch Lab, West Grove, PA) followed by treatment in avidin–biotin–peroxidase complex (ABC Elite; 1:1000; Vector Laboratories, Burlingame, CA) in 0.05M Tris buffer for 1 h at room temperature. Signal of Na^+/K^+ATPase was amplified with biotinylated tyramide for 10 min using the TSA amplification kit (Perkin Elmer Life and Analytical Sciences,

Waltham, MA) according to the manufacturer's instruction. The cells were incubated in Streptavidin Cy5 (1:250; Jackson Immunoresearch Lab) and Alexa 555 conjugated anti-rabbit IgG (1:500, Invitrogen) for 2h at room temperature. Sections were mounted on glass slides and coverslipped with Vechtashield Mounting medium (Vector). Imaging was performed on a Zeiss LSM 780 Confocal Microscope.

Ultrastructural studies

$2x10^5$ Thr92-D2^{HY} or Ala92-D2^{HY} stably expressing HEK-293 cells were plated on 2-well Permanox plastic chamber slides (Lab-Tek). The next day, cells were treated with 100uM CHX or DMSO as vehicle for 2h and fixed in chamber slides with the mixture of 3% PFA and 1% glutaraldehyde in 0.1M phosphate buffer (PB) pH7.4 (PB) at 37°C for 1h. After 3 washes for 2 min with 0.01M PBS pH 7.4, the cells were cryoprotected in 30% sucrose in PBS for 30 min at room temperature and then, quickly frozen over liquid nitrogen. The cells were washed again 3x with 0.01M PBS and then treated with 2% normal horse serum (NHS; in PBS) for 20 min. Pretreated cells were covered with rabbit anti-GFP serum (1:10,000) diluted in 2% NHS in PBS for 2 days at 4°C. After rinsing in PBS and in 0.1% cold water fish gelatin +1% bovine serum albumin (BSA) in PBS, the cells were incubated in donkey anti-rabbit IgG conjugated with 0.8 nm colloidal gold (Electron Microscopy Sciences, Fort Washington, PA) diluted at 1:100 in PBS containing 0.1% cold water fish gelatin and 1% BSA overnight at 4°C. After rinsing in PBS and fixed with 1.25% glutaraldehyde in 0.1M PB at room temperature for 10 min. After rinsing in PBS and in Aurion buffer for 20 min, gold particles were silver intensified using the Aurion R-Gent SE-LM Kit (Amersham–Pharmacia Biotech UK, Buckinghamshire, UK). The cells were washed 3x for 2 min in 0.2M sodium citrate, pH7.5 followed by washes in 0.1M PB. Cells were treated with 1% osmium tetroxide in 0.1M PB for 20 min at 4°C, followed by treatment with 2% uranyl acetate in 70% ethanol for 10 min. After dehydration in an ascending series of ethanol and acetonitrile, the cells were embedded in Durcupan ACM epoxy resin (Fluka) in a gelatin capsule, and polymerized at 56°C for 2 days. Serial 60–70 nm thick utlrasections were cut with Leica ultracut UCT ultramicrotome (Leica Microsystems, Wetzlar, Germany). The ultrathin

sections were mounted onto Formvar-coated single slot grids, contrasted with 2% lead citrate and examined with a Jeol-100 C transmission electron microscope.

Western blot quantitation

Western blot was performed as 30μg of total protein was resolved on a 4-12% SDS-PAGE gel. The samples were transferred to PVDF transfer membrane (Immobolin-FL, Millipore), incubated with various antibodies overnight at 4C and subsequently quantitated by using the LiCOR Odyssey instrument with Odyssey Image Studio software simultaneously (D2 vs. actin or tubulin) using different infrared channels.

Isolation of subcellular membrane fractions

Cells were collected, re-suspended in PBS solution with Complete-mini EDTA-free protease inhibitor (Roche) at 4°C. Cells were homogenized by 10 passages through a ball homogenizer (Isobiotec) at 10 μm clearance. Homogenates were centrifuged for 10 min at 800×*g*. The resulting nuclear (N′) pellet was washed twice with ice-cold PBS by centrifugation, while the supernatant fraction, containing cytosolic membranes and the cytosol, was designated as lysate and used for D2 activity assay. For western blot, nuclear and lysate samples were prepared using nonionic detergent Triton X-100. 293 cells were treated with 0.5% Triton X-100 at 4°C and centrifuged at 800×*g* for 10 min to isolate nuclear (N) fraction. The supernatant after centrifugation, which contained Triton X-100 soluble membranes and cytosol, was designated as lysate.

D2 activity assay

D2 activity was assayed in cell lysates and nuclear fractions using 150μg cell sonicated protein incubated in PE-EDTA pH 7.35 buffer at 37C in the presence of 1uM 125I-T4 and 20 uM DTT for 2h (19). Assay was terminated by addition of TCA and horse serum and 125I released quantified in a gamma counter. Background activity was measured for each sample in the presence of 100uM 125I-T4. Results are expressed as fmols 125I/min/mg protein.

Microarray studies of cultured cells

RNA was extracted from confluent cells from each group (RNeasy kit, Qiagen). Microarray data from samples from three plates each of the three cell types (YFP, Thr92-D2^{HY} and Ala92-D2^{HY}) were collected and analyzed as above. In addition, hierarchical clustering analysis was performed (HierarchicalClustering, GenePattern) using the pairwise average-linkage clustering method and Pearson correlation column distance measure to generate a dendogram. Creation and application of the class predictor (classifier) was performed (KNNXValidation, GenePattern) where the *k*-nearest-neighbors (KNN) class prediction algorithm was used to run class prediction iteratively against the dataset from all three cell genotypes. The PredictionResultsViewer and FeatureSummaryViewer modules were then used to obtain values for the absolute error rate (incorrect cases/total cases) and ROC error rate (receiver operating characteristic; fraction of true positives versus the fraction of false positives) and to view the genes comprising the classifier. To compare overlap between gene expression from the brain and cell microarray GSEAs, individual genes demonstrating core enrichment within the enriched gene sets were entered into VENNY (http://bioinfogp.cnb.csic.es/tools/venny/index.html*)* where Venn diagrams were used to identify common genes.

RT-qPCR

RT-qPCR (StepOnePlus Real-Time PCR Detection System, Applied Biosystems) using Taqman reagents (Applied Biosystems) was performed on human brain samples with the following conditions: 2 min at

50°C followed by 10 min at 95°C, 15 sec at 95°C, 1 min at 60°C x 40. Standard curves consisted of 5 points of serially diluted cDNA from all samples. Cyclophilin A (CycloA) was used as an internal control gene and there was no difference in CycloA expression between the three genotypes. The coefficient of correlation (r^2) was > 0.98 for all curves; amplication efficiency ranged from 90-110%. Results expressed as the ratio of target mRNA to CycloA mRNA. For HEK-293 cell PCR,18s was used for housekeeping.

In HeLa cells, BCL3 and SPOT14 were measured by RT-qPCR using SYBR green Fastmix (Quanta Bio-science) with the following conditions: 20 sec at 95°C, 3 sec at 95°C and 30 sec at 60°C x 40, and 15 sec at 95°C followed by 1 min at 60°C and 15 sec at 95°C. Standard curve, r^2 and amplification efficiency were as above

Statistics

All data were analyzed using PRISM software (GraphPad). Unless otherwise indicated, data represent mean ± SEM, comparisons between two groups were analyzed with a two-tailed Student's t test and comparisons between more than two groups were carried out by ordinary one-way ANOVA. A *p*-value <0.05 was considered significant.

Analysis of the human brain RT-qPCR data was done using Agilent Genespring GX version 12.6. The probeset data was $\log_2$ transformed and grouped according to Thr92-D2 homozygote, Het, and Ala92-D2 homozygous status. Each individual gene was compared using fold change between the three groups pairwise, selecting those genes that had an absolute fold change ≥ 1.5 in at least one of the three pairwise group comparisons. Each gene other than the mutant DIO2 was also correlated with DIO2 using Pearson's correlation. For clustering analysis, the data was further normalized to means of normal samples. This normalized gene expression data was clustered gene-wise using an unsupervised hierarchical clustering algorithm, with Euclidean distance metric and Ward's linkage rule.

Results

Analysis of the human brain transcriptome in patients carrying the Thr92-D2 polymorphism

The effects of the D2 polymorphism in humans were analyzed in the cerebral cortex of recently deceased adult accident/sudden death victims without known neurological or thyroid disease. Genotyping on brain samples from 95 donors revealed 24 homozygous for the Thr92AlaD2 polymorphism, 52 heterozygous and 25 normal patients; these frequencies are in Hardy-Weinberg equilibrium. Brain samples from 19 male Caucasian donors (six samples from homozygote Thr92-D2, seven heterozygotes and six homozygotes for Ala92-D2) were matched by age and BMI and chosen for further studies (Table S1). Homogenous samples from Brodmann's Area 38 of the temporal cortex were evaluated for gene expression. Given the diverse array of phenotypes exhibited by carriers of the polymorphism and the findings of normal catalytic activity of the D2 enzyme (27, 28), we hypothesized that this alteration could result in non-catalytic cellular consequences. Thus an unbiased whole-transcript microarray approach was used to assess the potential impact of the polymorphism and generate hypotheses regarding the mechanism of dysfunction in Ala92-D2 expression.

First, differentially expressed individual genes were identified by comparing the data from three genotypes: Ala92-D2 homozygotes vs. Thr92-D2 homozygotes, Ala92-D2 homozygotes vs. heterozygotes (Het), and Hets vs. Thr92-D2 homozygotes. Differences in gene expression between the Ala92-D2 homozygote vs. Thr92-D2 homozygote comparison were considered at a p-value <0.05 (Fig. 1A). As a result, 839 named genes were found to be differentially expressed where 110 of these were altered at a fold change >1.3 or <-1.3 (Table S2). A heat map incorporating the 25 genes with the highest or lowest expression values by fold change between these two genotypes was built (Fig. 1B); it is notable that despite

statistical significance between the two genotypes, the expression of some genes is heterogeneous reflecting their multifactorial regulation.

In order to evaluate the physiologic context of the transcriptional footprint left by Ala92-D2-expression, the microarray data were then analyzed by GSEA (29, 30). When performed in the Ala92-D2 vs. Thr92-D2 samples, GSEA revealed enrichment of 18 gene sets at a nominal p-value <0.05 (3 of which were additionally enriched at an FDR <0.25) and downregulation of 10 gene sets at a nominal p-value <0.05 (Table S3). Within these gene sets a total of 382 genes demonstrated core enrichment; heat map of the 50 top genes for each phenotype was generated (Fig. 1C). Investigator analysis of transcripts identified by GSEA showed that genes enriched in Ala92-D2 homozygotes were primarily related to apoptosis, oxidation-reduction, mitochondrial function, carbohydrate metabolism, ribosome components, inflammation, lipid/fatty acid metabolism, cytoskeleton structure, Golgi/ER transport, DNA repair and transcription regulation. Genes downregulated in Ala92-D2 homozygotes were related to cell growth, cell cycle control, phospholipid maintenance, EGFR signaling, phosphatidylinositol and lipoprotein metabolism.

To test whether carriers of the Ala92-D2 genotype exhibited changes in TH signaling we examined microarray data for the expression level of a set of typical T3-responsive genes (Table S4) (18, 19) and found no significant differences by GSEA (Fig. S1A). Next, expression data were processed through pathway analysis software to identify cellular pathways that altered at the $p<0.05$ level when the three genotypes are assessed. Many of the top pathways exhibiting significant changes in at least 60% of their genes shared overlapping functional significance (Fig. 1D); Huntington's Disease Signaling was the top canonical pathway identified (ratio of genes affected 180/225, p-value <0.0001).

A cell model to assess the impact of Thr92-D2 expression

Findings from the human brain microarray supported an association between gene expression pattern and genotype and thus served as grounds for further investigation using a cell model. HEK-293 cells were chosen as suitable candidates for the model as they exhibit many features of neuronal lineage (22, 23) and are known for lacking in deiodinase expression (20); these cells also lack in TR, which eliminates cell changes due to altered TH signaling (21). Thus, we used a previously characterized HEK-293 cell model that stably expresses a His/YFP-doubled tagged Sec133Cys-Thr92D2 (Thr92-D2^{HY}) (24). In this setting, Thr92-D2^{HY} exhibited similar cellular properties as endogenously expressed D2 and the host cells were not adversely affected when compared to cells stably expressing YFP (24). Here we observed that stable expression of Ala92-D2^{HY} protein also did not result in gross cellular phenotypic alterations (Fig. 2A-B). Ala92-D2^{HY} sorted predominantly to the ER and no differences were observed in cell size as assessed by flow cytometry (Fig. S2A-B), cell cycle (Fig. S2C) or cell duplication time (Fig. S2D) when compared with cells stably expressing Thr92-D2^{HY}.

Both Thr92-D2^{HY} and Ala92-D2^{HY} are found in the nucleus and ER but only Ala92-D2^{HY} has a longer half-life and can be found in the Golgi apparatus

The Thr for Ala substitution in the D2 molecule is in the instability loop (5, 6), possibly affecting D2 turnover rate and other functions of Ala92-D2^{HY}-expressing cells. Thus, we first looked at the rate of disappearance of Ala92-D2^{HY} protein following exposure to its natural substrate T4 that accelerates D2 ubiquitination and proteasomal degradation (31). Notably, whereas there was progressive loss of Thr92-D2^{HY} after T4 was added to the medium, the abundance of the Ala92-D2^{HY} protein remained largely unaffected by T4, suggesting impaired ubiquitination/degradation (Fig. S3A-B). Indeed, we used cycloheximide (CHX) to arrest protein synthesis and found that Ala92-D2^{HY} had a longer half-life (~33 vs. ~13 min) when compared to Thr92-D2^{HY} protein (Fig. 2C-D). This was confirmed with immunofluorescent localization where more Ala92-D2^{HY} protein is seen after CHX treatment (Fig. 2E-F).

A more detailed analysis of the immunofluorescence microscopy images shows that $D2^{HY}$ protein can also be found closely associated with the nucleus (Fig. 2A-B). In fact, when stained for nuclear lamin (Fig. S3E-F), co-localization of $D2^{HY}$ proteins was demonstrated but no differences were observed between Thr92-D2 and Ala92-D2 proteins (Pearson's coefficient: 0.48 ± 0.02 vs. 0.49 ± 0.03; n=10). The presence of D2 in the ER and nucleus was also detected using EM, but no differences were observed between Thr92-D2 and Ala92-D2 proteins in these cellular compartments (Fig. 2G-J). Next we isolated the nuclear fraction and detected Thr92-D2 and Ala92-D2 proteins by western analysis, both types of D2 disappearing with CHX treatment (Fig. S3C). Notably, nuclear D2 is catalytically active where its activity is not influenced by the polymorphism (Fig. S3D).

A remarkable new finding of the present studies is the observation with EM that only Ala92-$D2^{HY}$ could be identified in the Golgi apparatus (Fig. 3A-C). Even when cells are depleted of D2 by treatment with CHX, D2 was still consistently observed in the membranes of the Golgi apparatus (Fig. S4). Structural differences in Golgi as assessed by immunofluorescence were apparent under these conditions with Golgi in Ala92-$D2^{HY}$-expressing cells exhibiting a circular configuration as opposed to its normal ribbon morphology (Fig. 3D-F). These findings were also documented by EM but only when the Golgi apparatus in Ala92-$D2^{HY}$-expressing cells was further stressed with BFA treatment (Fig. 3G-I, M-O).

Defining a transcriptional fingerprint of Ala92-$D2^{HY}$ expression in cultured cells

Given that fundamental biological differences exist between Thr92-$D2^{HY}$ and Ala92-$D2^{HY}$ that could underlie the transcriptional patterns observed in affected human brains, we next turned to an unbiased microarray approach to assess the impact of Ala92-$D2^{HY}$ expression in our cell model. Differential expression analysis was performed to identify individual genes altered in the three cell lines: Ala92- $D2^{HY}$ vs. Thr92- $D2^{HY}$, Ala92- $D2^{HY}$ vs. YFP, Thr92 $D2^{HY}$ vs. YFP. A volcano plot for Ala92- $D2^{HY}$- vs. Thr92- $D2^{HY}$-expressing cells allowed for visualization of the differences in gene expression at a p-value <0.05

(Fig. 4A). This resulted in 3155 named genes differentially expressed where 263 of these were altered at a fold change >1.3 or <-1.3 (Table S5). The 50 most affected genes by the Ala92-D2^{HY} expression were plotted in a heat map (Fig. 4B).

We then performed a hierarchical clustering analysis (32). The resulting dendogram utilized the expression profiles of 6643 genes within these phenotypic contexts and indicated that the gene expression pattern appropriately clustered the three samples in groups with their respective phenotypes and that Ala92-D2 and Thr92-D2 clusters exhibited a more similar gene expression pattern than the YFP controls (Fig. 4C). Also, we used class prediction analysis of the microarray dataset to create and evaluate a genetic classifier using the KNN class prediction method (Table S6). Utilization of this classifier on the cell microarray data correctly classifies 9/9 samples (0 absolute error, 0 ROC error, confidence of prediction of each sample 0.667).

In order to evaluate the physiologic context of the transcriptional footprint left by Ala92-D2^{HY}-expression, the microarray data were analyzed by GSEA (29, 30), which revealed 97 gene sets enriched at a nominal p-value of <1% in Ala92-D2^{HY}- vs. Thr92-D2^{HY}-expressing cells (Table S7). Subsequent investigator analysis indicated that a predominance of the genes contained in these sets played a role in NF-κB signaling, inflammation, lysosome, cell cycle control, DNA repair and cytoskeleton maintenance. Twenty-nine of these gene sets contain genes involved in cell membrane transport or function (Table S7). There were 63 gene sets downregulated in Ala92-D2^{HY}-expressing cells that were involved in DNA metabolism, cell cycle maintenance, transcription regulation, apoptosis, EGFR signaling and mitochondria (Table S6). A GSEA-generated heat map of the top 50 genes (up and down) by their ranking criteria was obtained (Figure 4D).

Next we tested whether differences between Ala92-D2- versus Thr92-D2 could interfere with TH signaling by measuring the expression level of a custom set of typical T3-responsive genes (Table S4) (18, 19)

and, as in the brains, found no significant differences by GSEA (Fig. S1B). Differences in TH activation between Ala92-D2- versus Thr92-D2 were also evaluated using a previously characterized co-culture system (33) where T3-responsive cells were co-cultured with Thr92-D2^{HY}- or Ala92-D2^{HY}-expressing cells. Here HeLa cells were used as targets as they express two highly sensitive T3-responsive genes, i.e. BCL3 or SPOT14 (34, 35), but no differences in the expression of either gene were observed in co-cultures with either Thr92-D2^{HY}- or Ala92-D2^{HY}-expressing cells (Fig. S5).

Are the genes identified in the cells also altered in the human brain samples obtained from Ala92-D2 homozygous donors?

To that end we generated a list of 40 genes (40-list) identified in the cell microarray GSEA based on their representation within prominent gene ontology classes and analyzed their expression level in all brain samples by RT-qPCR. CDK2 expression inversely correlated with the Ala92-D2 allele dose (Fig. 5A) whereas the opposite was observed for CD24 (Fig. 5B). Next, we combined expression data of Hets and Ala92-D2 homozygotes to test whether the expression of these 40 genes was indistinctly affected by at least one copy of the AlaD2 allele. This strategy confirmed that 9 other genes identified in the cells, totaling 11 genes (11-list), were affected by the AlaD2 allele in the human brain (Fig. 5C). The 40-list was further analyzed using the fold change ranking approach (36) that yielded 21 genes (7 genes in common with the 11-list) with expression level that varied >1.5-fold between any two genotypes (Fig. 5D) and clustered into 5 groups (Fig. 5E).

Next, we asked whether the expression of any of the genes in the 40-list correlated with the level of D2 expression within each genotype. Using the Pearson correlation analysis we identified 27 genes that significantly correlated with the D2 mRNA level within samples of each of the three genotypes (Table S8; Fig. 5F). Notably, only the thyroid hormone transporter gene SLCO1C1 (OATP14) expression correlated significantly with D2 mRNA independently of genotype (Fig. 5F).

Using human brain and cell microarray data to define the Ala92-D2 genetic fingerprint

Venn diagrams were used to identify common genetic features between human brain and cell microarray datasets. We first looked at individual genes enriched in the gene sets from cell- (1228 genes) and human brain- (382 genes) GSEA and identified 79 common genes (79-list) (Fig. 5G). Notably, the gene set for Epidermal Growth Factor Receptor Signaling Pathway (EGFR) was down-regulated in human brain homozygous for Ala92-D2 and Ala92-D2-expressing cells (Tables S3,S7; Fig. S6).

Next, a classifier of the 79-list was created and applied to the microarray data sets from the Thr92-D2 and Ala92-D2 homozygous human brain donors to predict their genotype; all of the Thr92-D2 samples were correctly classified as well as 5/6 Ala92-D2 samples. When this classifier was strengthened with the addition of two genes identified from a computer-generated weighted voting prediction model, SNORD16 and TRAPPC4 (Table S2), the 81-gene classifier correctly predicted the genotypes of all homozygous Thr92-D2 and Ala92-D2 human brain samples (0 absolute error, 0 ROC error, confidence of prediction of each sample 0.028-0.704). We also applied the 81-gene classifier to the data set of all 19 samples to predict carrier status of at least one allele, which was correct in 18 patients (Absolute error 0.05, ROC error 0.04).

Oxidative stress plays a role in the genetic fingerprint of Ala92-D2^{HY}-expressing cells

Next we used the cell model to assess findings obtained in the combined genetic analysis of brain and cell microarrays, such as Golgi function and oxidative stress (Fig. 1D; Tables S3,S7). We looked at the expression of seven genes affected by the Ala92-D2^{HY} before (Fig. 6A) and after treatment with the chemical chaperone TMAO (minimizes ER stress; Fig. 6B) or the anti-oxidant NAC (Fig. 6C). Here, we also included a subset of five Golgi apparatus related genes given the ectopic presence of Ala92-D2^{HY} in this

structure and the finding of three Golgi-specific genes (ATP11B, ABCG1, TRAPPC4) and 15 Golgi-related genes (Fig. 5G) in the 81-gene list. Whereas treatment with TMAO for 24 h normalized expression of only one of those genes (Fig. 6C), exposure to NAC had a more consistent pattern of abating differences between Ala92-D2^{HY} and Thr92-D2^{HY}-expressing cells in 5 of the 7 genes analyzed, all related to the Golgi apparatus (Fig. 6C). Notably, the observation that Ala92-D2^{HY} expressing cells exhibit an increase in the pre-apoptosis marker Annexin-V (Fig. 6D) also points towards oxidative stress as well as disruption in the EGFR signaling pathway (37), similar to what was observed in EGFR$^{-/-}$ cortical astrocytes (38).

Discussion

A striking observation in the human brain and cell models is that expression of Ala92-D2 interferes with basic cellular processes in a pattern that establishes an 81-gene fingerprint of transcriptional alterations related to CNS diseases, ubiquitin and ER stress, mitochondrial dysfunction, inflammation, apoptosis, DNA repair and growth factor signaling. It is conceivable that the change in the single amino acid produces a protein that upsets basic ER functions triggering ER stress and changes in ubiquitination genes; the Ala92-D2 ultimately escapes to the Golgi apparatus and disrupts its normal ribbon morphology. Thus mitochondrial dysfunction, inflammation and apoptosis are likely consequences of primary disruption in ER and Golgi. The prolonged half-life exhibited by Ala92-D2^{HY} could also be a consequence of its presence in the Golgi, sheltered from the typical proteasomal machinery present in its native ER location. It is notable that treatment with an anti-oxidant agent normalized the expression of multiple genes affected by Ala92-D2^{HY}, indicating that oxidative stress plays a role in defining the genetic fingerprint. Thus, it is plausible that this fingerprint underlies the different clinical phenotypes associated with homozygosity for Ala92-D2.

Another striking observation in the present studies was that both native and polymorphic D2 were found associated with the nuclear compartment in the HEK-293 cells. Of course this could be the result of D2 overexpression in this cell model and final determination awaits the development of high-quality D2 antisera to study endogenous D2 expression. If confirmed *in vivo*, this would explain the decades-old kinetic and physiological data that D2-generated T3 contributes much to the occupation of TR (39, 40). In the brain of course, D2 is expressed in glial cells while TR is expressed predominantly in neurons and thus a higher level of TR occupancy is most likely the result of accelerated local T3 production and signaling through a paracrine mechanism (33). In any event, that no differences in nuclear D2 were observed between Thr92-D2^{HY} and Ala92-D2^{HY} proteins support the notion that TH signaling is not grossly affected by this polymorphism (Fig. S3C-D).

A strength of the present study is the complementary usage of microarray analysis in brain and cells, which led to the refinement of the genetic fingerprint initially discovered in the brains. The resulting 81-gene fingerprint was highly efficacious as a genotype classifier in these samples. Along these lines, the observation that Huntington's disease was the top pathway identified in the gene analysis of the human brains indicates similarities between the two diseases might exist. Indeed, Huntington's is a CNS degenerative disease that causes chorea and loss of cognition that is caused by huntingtin, an ER-associated protein that normally translocates to and from the cell nucleus (41). Carriers of the mutant huntingtin gene express an abnormally long version of the huntingtin protein that is hydrolyzed into smaller peptides that accumulate and disrupt the normal function of neurons. This leads to ER and oxidative stress, and eventually to apoptosis of neurons in the striatum, explaining the signs and symptoms of Huntington's disease (42, 43). While it is too early to draw any definitive conclusions, the parallels between the Huntington's disease mechanism and the observations in our Ala92-D2^{HY} cell model are intriguing and could ultimately indicate that carriers for the D2 variant may be predisposed to neurodegenerative processes. The gene analyses also point towards alternative disease mechanisms such as disruption of the EGF signaling pathway, which is known for playing a role in cognitive development (12) and impairment in diseases including Parkinson's (14, 15), Alzheimer's (16) and schizophrenia (13).

It is clear that the clinical phenotypes associated the Ala92-D2 polymorphism are not limited to hypothyroid patients, but can be traced back to tissues/organs that express D2 (44). However, it is unclear why hypothyroid carriers of the Ala92-D2 polymorphism would prefer combination therapy with L-T4 and L-T3 (7) given that TH signaling is not affected by Ala92-D2. While much additional investigation is still needed, it is conceivable that compensatory mechanisms developed in carriers of the Ala92-D2 polymorphism lose effectiveness in the setting of treatment with L-T4, when patients exhibit an elevation in serum T4/T3 ratio (45, 46). On this note, D2 mRNA levels in the brain correlate with the TH transporter

OATP14 (Fig. 5F). Therefore, the present findings do not provide a direct rationale for combination therapy with L-T4 and L-T3.

In conclusion, we have uncovered a unique 81-gene fingerprint left in the brain and in cells expressing Ala92-D2. This is caused by cellular accumulation of Ala92-D2 that can be found ectopically in the Golgi apparatus, and is associated with ER and oxidative stress as well as pre-apoptosis. There are striking similarities between these findings and changes observed in other well-characterized brain degenerative diseases. Future research should clarify whether the disease mechanisms proposed in the present investigation contribute to the phenotype of Ala92-D2 carriers.

Acknowledgements

We thank Selmar Leeuwenburgh for assistance with genotyping and Katelyn Hughes for assistance with performance of microarray studies. This work was supported by grants from the National Institute of Diabetes and Digestive Kidney Diseases, the Hungarian Brain Research Program and the Lendület grant of the Hungarian Academy of Sciences. The University of Miami Brain Endowment Bank is funded in part with Federal funds from the NIMH, NINDS and NICHD, National Institutes of Health, Department of Health and Human Services, under Contract No. HHSN271201300028C.

References

1. Golden SH, Robinson KA, Saldanha I, Anton B, Ladenson PW**.** Clinical review: Prevalence and incidence of endocrine and metabolic disorders in the United States: a comprehensive review. J Clin Endocrinol Metab. 2009;94(6):1853-78.

2. Canaris GJ, Manowitz NR, Mayor G, Ridgway EC**.** The Colorado thyroid disease prevalence study. Archives of Internal Medicine. 2000;160(4):526-34.

584 3. Wiersinga WM, Duntas L, Fadeyev V, Nygaard B, Vanderpump MP**.** 2012 ETA Guidelines: The
585 Use of L-T4 + L-T3 in the Treatment of Hypothyroidism. Eur Thyroid J. 2012;1(2):55-71.
586 4. Dora JM, Machado WE, Rheinheimer J, Crispim D, Maia AL**.** Association of the type 2
587 deiodinase Thr92Ala polymorphism with type 2 diabetes: case-control study and meta-analysis. Eur J
588 Endocrinol. 2010;163(3):427-34.
589 5. Dentice M, Bandyopadhyay A, Gereben B, Callebaut I, Christoffolete MA, Kim BW, et al. The
590 Hedgehog-inducible ubiquitin ligase subunit WSB-1 modulates thyroid hormone activation and PTHrP
591 secretion in the developing growth plate. Nat Cell Biol. 2005;7(7):698-705.
592 6. Callebaut I, Curcio-Morelli C, Mornon JP, Gereben B, Buettner C, Huang S, et al. The
593 iodothyronine selenodeiodinases are thioredoxin-fold family proteins containing a glycoside hydrolase
594 clan GH-A-like structure. J Biol Chem. 2003;278(38):36887-96.
595 7. Panicker V, Saravanan P, Vaidya B, Evans J, Hattersley AT, Frayling TM, et al. Common
596 variation in the DIO2 gene predicts baseline psychological well-being and response to combination
597 thyroxine plus triiodothyronine therapy in hypothyroid patients. J Clin Endocrinol Metab.
598 2009;94(5):1623-9.
599 8. Guo TW, Zhang FC, Yang MS, Gao XC, Bian L, Duan SW, et al. Positive association of the
600 DIO2 (deiodinase type 2) gene with mental retardation in the iodine-deficient areas of China. J Med
601 Genet. 2004;41(8):585-90.
602 9. Taylor P OO, Sayers A, Pearce E, Gregory J, Lazarus J, Panicker V, Channon S, Timpson N,
603 Dayan C**.** Effect of low thyroid hormone bioavailability on childhood cognitive development: data from
604 the Avon Longitudinal Study of Parents and Children birth cohort. The Lancet. 2014;383:S100.
605 10. He B, Li J, Wang G, Ju W, Lu Y, Shi Y, et al. Association of genetic polymorphisms in the type
606 II deiodinase gene with bipolar disorder in a subset of Chinese population. Prog Neuropsychopharmacol
607 Biol Psychiatry. 2009;33(6):986-90.

11. Wang X, McCullough KD, Franke TF, Holbrook NJ. Epidermal growth factor receptor-dependent Akt activation by oxidative stress enhances cell survival. J Biol Chem. 2000;275(19):14624-31.

12. Futamura T, Kakita A, Tohmi M, Sotoyama H, Takahashi H, Nawa H. Neonatal perturbation of neurotrophic signaling results in abnormal sensorimotor gating and social interaction in adults: implication for epidermal growth factor in cognitive development. Mol Psychiatry. 2003;8(1):19-29.

13. Kao WT, Wang Y, Kleinman JE, Lipska BK, Hyde TM, Weinberger DR, et al. Common genetic variation in Neuregulin 3 (NRG3) influences risk for schizophrenia and impacts NRG3 expression in human brain. Proc Natl Acad Sci U S A. 2010;107(35):15619-24.

14. Pellecchia MT, Santangelo G, Picillo M, Pivonello R, Longo K, Pivonello C, et al. Serum epidermal growth factor predicts cognitive functions in early, drug-naive Parkinson's disease patients. J Neurol. 2013;260(2):438-44.

15. Chen-Plotkin AS, Hu WT, Siderowf A, Weintraub D, Goldmann Gross R, Hurtig HI, et al. Plasma epidermal growth factor levels predict cognitive decline in Parkinson disease. Ann Neurol. 2011;69(4):655-63.

16. Marksteiner J, Kemmler G, Weiss EM, Knaus G, Ullrich C, Mechtcheriakov S, et al. Five out of 16 plasma signaling proteins are enhanced in plasma of patients with mild cognitive impairment and Alzheimer's disease. Neurobiol Aging. 2011;32(3):539-40.

17. Zevenbergen C, Klootwijk W, Peeters RP, Medici M, de Rijke YB, Huisman SA, et al. Functional Analysis of Novel Genetic Variation in the Thyroid Hormone Activating Type 2 Deiodinase. J Clin Endocrinol Metab. 2014:jc20142281.

18. Hernandez A, Morte B, Belinchon MM, Ceballos A, Bernal J. Critical role of types 2 and 3 deiodinases in the negative regulation of gene expression by t3 in the mouse cerebral cortex. Endocrinology. 2012;153(6):2919-28.

19. Bianco AC, Anderson G, Forrest D, Galton VA, Gereben B, Kim BW, et al. American thyroid association guide to investigating thyroid hormone economy and action in rodent and cell models. Thyroid. 2014;24(1):88-168.

20. Zeold A, Doleschall M, Haffner MC, Capelo LP, Menyhert J, Liposits Z, et al. Characterization of the nuclear factor-kappa B responsiveness of the human dio2 gene. Endocrinology. 2006;147(9):4419-29.

21. Zhang C, Kim S, Harney JW, Larsen PR**.** Further characterization of thyroid hormone response elements in the human type 1 iodothyronine deiodinase gene. Endocrinology. 1998;139:1156-63.

22. Thomas P, Smart TG**.** HEK293 cell line: a vehicle for the expression of recombinant proteins. J Pharmacol Toxicol Methods. 2005;51(3):187-200.

23. Shaw G, Morse S, Ararat M, Graham FL**.** Preferential transformation of human neuronal cells by human adenoviruses and the origin of HEK 293 cells. FASEB J. 2002;16(8):869-71.

24. Arrojo EDR, Egri P, Jo S, Gereben B, Bianco AC**.** The type II deiodinase is retrotranslocated to the cytoplasm and proteasomes via p97/Atx3 complex. Mol Endocrinol. 2013;27(12):2105-15.

25. Jo S, Kallo I, Bardoczi Z, Arrojo EDR, Zeold A, Liposits Z, et al. Neuronal hypoxia induces hsp40-mediated nuclear import of type 3 deiodinase as an adaptive mechanism to reduce cellular metabolism. J Neurosci. 2012;32(25):8491-500.

26. Kallo I, Mohacsik P, Vida B, Zeold A, Bardoczi Z, Zavacki AM, et al. A novel pathway regulates thyroid hormone availability in rat and human hypothalamic neurosecretory neurons. PLoS One. 2012;7(6):e37860.

27. Canani LH, Capp C, Dora JM, Meyer EL, Wagner MS, Harney JW, et al. The type 2 deiodinase A/G (Thr92Ala) polymorphism is associated with decreased enzyme velocity and increased insulin resistance in patients with type 2 diabetes mellitus. J Clin Endocrinol Metab. 2005;90(6):3472-8.

28. Peeters RP, van Toor H, Klootwijk W, de Rijke YB, Kuiper GG, Uitterlinden AG, et al. Polymorphisms in thyroid hormone pathway genes are associated with plasma TSH and iodothyronine levels in healthy subjects. The Journal of Clinical Endocrinology and Metabolism. 2003;88(6):2880-8.

29. Subramanian A, Tamayo P, Mootha VK, Mukherjee S, Ebert BL, Gillette MA, et al. Gene set enrichment analysis: a knowledge-based approach for interpreting genome-wide expression profiles. Proc Natl Acad Sci U S A. 2005;102(43):15545-50.

30. Mootha VK, Lindgren CM, Eriksson KF, Subramanian A, Sihag S, Lehar J, et al. PGC-1alpha-responsive genes involved in oxidative phosphorylation are coordinately downregulated in human diabetes. Nat Genet. 2003;34(3):267-73.

31. Sagar GD, Gereben B, Callebaut I, Mornon JP, Zeold A, da Silva WS, et al. Ubiquitination-induced conformational change within the deiodinase dimer is a switch regulating enzyme activity. Mol Cell Biol. 2007;27(13):4774-83.

32. Reich M, Liefeld T, Gould J, Lerner J, Tamayo P, Mesirov JP. GenePattern 2.0. Nat Genet. 2006;38(5):500-1.

33. Freitas BC, Gereben B, Castillo M, Kallo I, Zeold A, Egri P, et al. Paracrine signaling by glial cell-derived triiodothyronine activates neuronal gene expression in the rodent brain and human cells. J Clin Invest. 2010;120(6):2206-17.

34. Sharma D, Fondell JD. Temporal formation of distinct thyroid hormone receptor coactivator complexes in HeLa cells. Mol Endocrinol. 2000;14(12):2001-9.

35. Sharma D, Fondell JD. Ordered recruitment of histone acetyltransferases and the TRAP/Mediator complex to thyroid hormone-responsive promoters in vivo. Proc Natl Acad Sci U S A. 2002;99(12):7934-9.

36. Consortium M, Shi L, Reid LH, Jones WD, Shippy R, Warrington JA, et al. The MicroArray Quality Control (MAQC) project shows inter- and intraplatform reproducibility of gene expression measurements. Nat Biotechnol. 2006;24(9):1151-61.

37. Kang N, Zhang JH, Qiu F, Tashiro S, Onodera S, Ikejima T. Inhibition of EGFR signaling augments oridonin-induced apoptosis in human laryngeal cancer cells via enhancing oxidative stress coincident with activation of both the intrinsic and extrinsic apoptotic pathways. Cancer Lett. 2010;294(2):147-58.

38. Wagner B, Natarajan A, Grunaug S, Kroismayr R, Wagner EF, Sibilia M**.** Neuronal survival depends on EGFR signaling in cortical but not midbrain astrocytes. EMBO J. 2006;25(4):752-62.

39. Gereben B, Zavacki AM, Ribich S, Kim BW, Huang SA, Simonides WS, et al. Cellular and molecular basis of deiodinase-regulated thyroid hormone signaling. Endocr Rev. 2008;29(7):898-938.

40. Silva JE, Dick TE, Larsen PR**.** The contribution of local tissue thyroxine monodeiodination to the nuclear 3,5,3'-triiodothyronine in pituitary, liver, and kidney of euthyroid rats. Endocrinology. 1978;103(4):1196-207.

41. Atwal RS, Xia J, Pinchev D, Taylor J, Epand RM, Truant R**.** Huntingtin has a membrane association signal that can modulate huntingtin aggregation, nuclear entry and toxicity. Hum Mol Genet. 2007;16(21):2600-15.

42. Labbadia J, Morimoto RI**.** Huntington's disease: underlying molecular mechanisms and emerging concepts. Trends Biochem Sci. 2013;38(8):378-85.

43. Vidal R, Caballero B, Couve A, Hetz C**.** Converging pathways in the occurrence of endoplasmic reticulum (ER) stress in Huntington's disease. Curr Mol Med. 2011;11(1):1-12.

44. Bianco AC, Casula S**.** Thyroid Hormone Replacement Therapy: Three 'Simple' Questions, Complex Answers. European Thyroid Journal. 2012;1:88-98.

45. Gullo D, Latina A, Frasca F, Le Moli R, Pellegriti G, Vigneri R**.** Levothyroxine monotherapy cannot guarantee euthyroidism in all athyreotic patients. PLoS One. 2011;6(8):e22552.

46. Stock JM, Surks MI, Oppenheimer JH**.** Replacement dosage of L-thyroxine in hypothyroidism. A re-evaluation. N Engl J Med. 1974;290(10):529-33.

Figure Legends

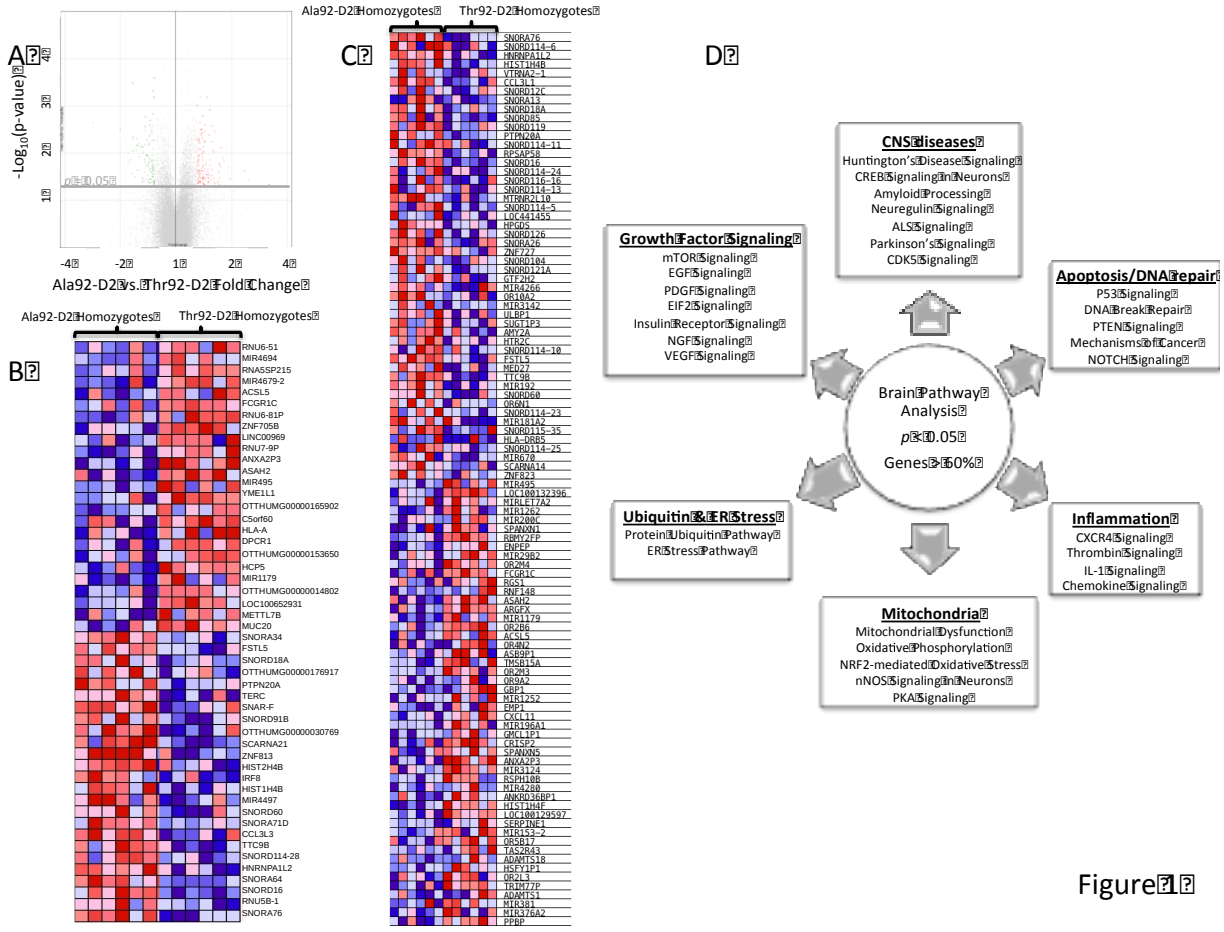

Figure 1

Figure 1. Microarray analysis of human brain from patients homozygous and heterozygous for the Thr92AlaD2 polymorphism. (A) Volcano plot of expression data in the comparison of Ala92-D2 (n = 6) and Thr92-D2 (n = 6) homozygotes; highlighted genes are significant at a *p*-value < 0.05 and a fold change > 1.3 (red) or < -1.3 (green). Generated in Affymetrix Transcriptome Analysis Console; (B) Heat map of the 25 most enriched and 25 most down-regulated genes in human brain samples from Ala92-D2 and Thr92-D2 homozygotes by fold change from differential expression analysis; expression values are represented as colors (red: increased expression; blue decreased expression) with the degree of color saturation indicating degree of expression; distinct transcriptional trends are observed; (C) Heat map of the top 50 features exhibited by polymorphic homozygotes versus normal patients as calculated in the gene set enrichment analysis software; (D) Canonical pathways identified in analysis of all brain samples (n =

19) where individual pathways are grouped by overlap in function, each of these pathways was altered at $p<0.05$ and with a ratio of genes affected within the pathway >60%.

Figure 2

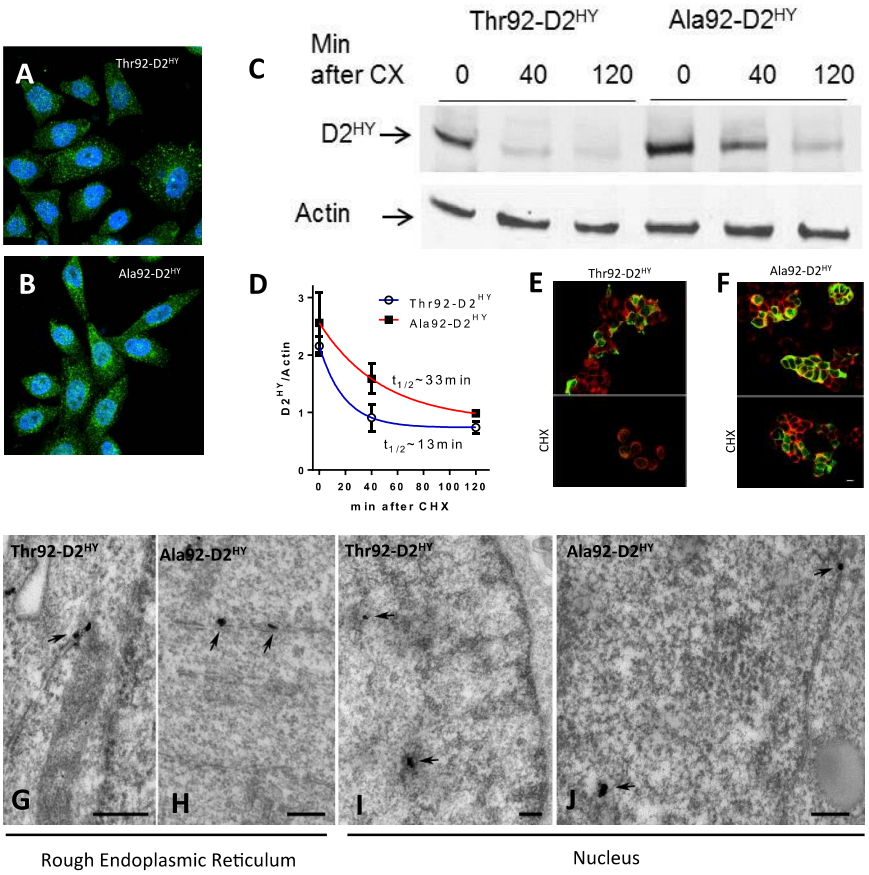

Figure 2. Thr92-D2^{HY} and Ala92-D2^{HY} are both found in the nucleus but Ala92-D2^{HY} has a longer half-life. (A-B) Immunofluorescence of HEK-293 cells stably expressing D2^{HY} proteins; D2 was stained with □YFP (green) and is found throughout the ER; nuclei were stained with DAPI (blue); (C) the indicated cells were incubated for 40-120 min with 100 uM CHX and subsequently harvested and processed for western analysis using □YFP and □Actin; (D) quantification of the bands shown in **C**; data were analyzed by non-linear regression assuming that D2 decays exponentially after addition of CHX; all data are the mean ± SEM of 3 entries per data-point; (E-F) immunofluorescent detection of plasma membrane by the Na^+/K^+-ATPase (red) and αYFP of D2^{HY} fusion proteins (green) in the same cells as A-B before (above) and after (below) treatment with CHX for 120 min; (G) electron microscopy of HEK-293 cells

stably expressing D2^{HY} proteins as in **A-B**; silver grains denoting D2^{HY} can be visualized in the rough endoplasmic reticulum (arrows) in both Thr92-D2^{HY} and (H) Ala92-D2^{HY}-expressing cells; (I) the nucleus also contains Thr92-D2^{HY} and (J) Ala92-D2^{HY} proteins; scale bars = 0.25 um.

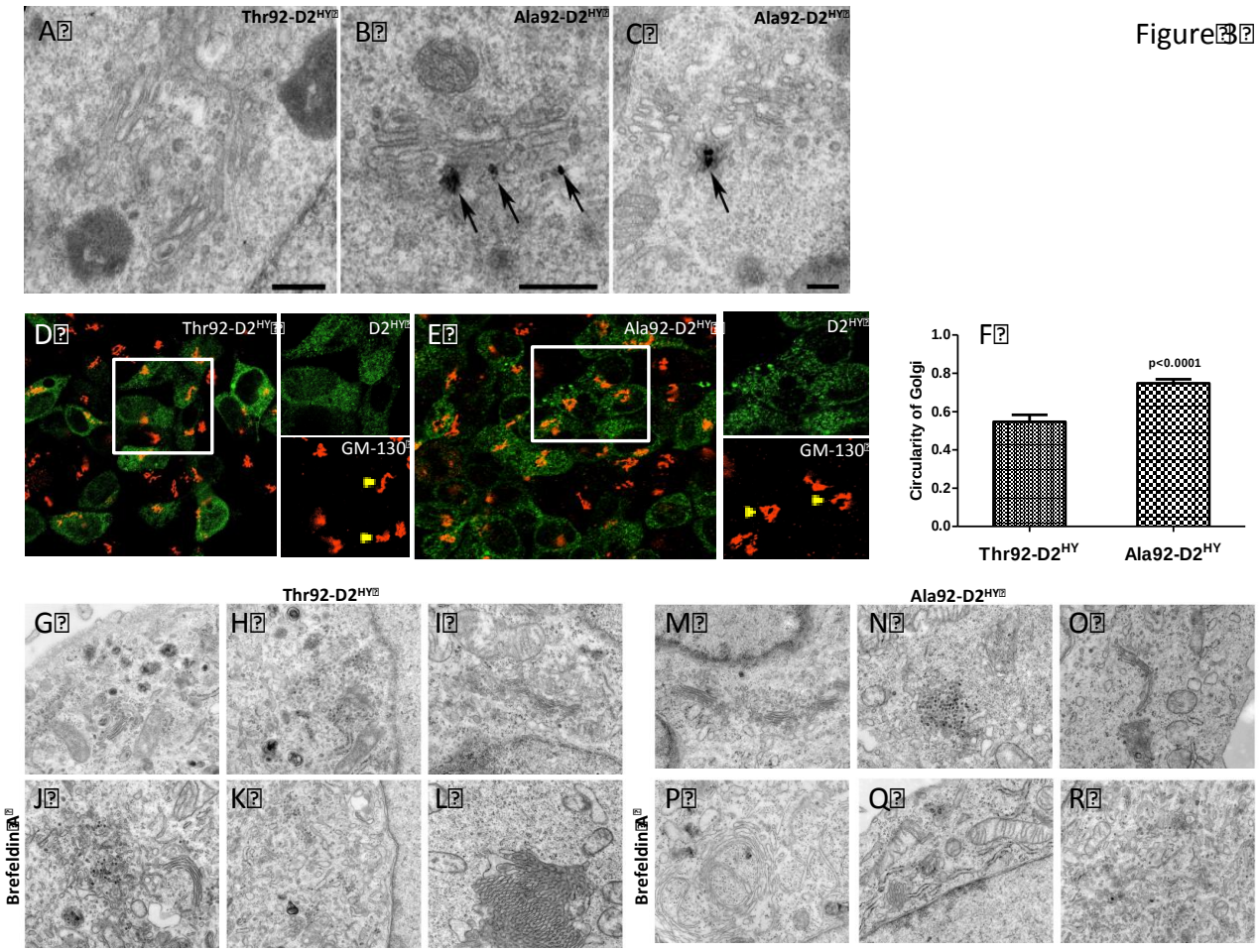

Figure 3

Figure 3. Ala92-D2^{HY}, but not Thr92-D2^{HY}, can be found in the Golgi. (A) Electron microscopy of Thr92-D2^{HY} expressing cells where a typical Golgi apparatus is devoid of D2 protein; (B-C) same as **A** except that Ala92-D2^{HY} expressing cells were studied; in this case, silver grains denoting the presence of Ala92-D2^{HY} protein are observed associate to the Golgi apparatus (arrow); scale bars = 0.25 um; (D) Immunofluorescence staining of Thr92-D2^{HY} and (E) Ala92-D2^{HY} (green) expressing cells with cis-Golgi marker GM-130 (red). White box is enlarged in green (D2) and red (GM-130) channels. Yellow arrows show Thr92-D2^{HY} and Ala92-D2^{HY} specific cis-Golgi staining features, where Ala92-D2^{HY} Golgi demonstrates a circular morphology compared to the ribbon configuration in the Thr92-D2^{HY}-expressing cells;

(F) The circularity index of the cis-Golgi complex in individual D2^{HY}-expressing cells was measured in ImageJ where the cis-Golgi structure in Ala92-D2^{HY} cells had higher circularity values than from Thr92-D2^{HY} cells; (G-I, M-O) Untreated cells display the typical appearance of Golgi-complex independently from the type of D2 expressed in the cells. The cisternae of the Golgi complex were organized in parallel, slightly curved and surrounded by small Golgi vesicles; (J-L) In cells expressing the Thr92-D2^{HY}, BFA treatment (0.5 µg/ml) resulted in a disorganization of the Golgi apparatus with scattered, dilated and short cisternae. However, some organized Golgi can be observed; (P-R) In BFA-treated Ala92D2^{HY}-expressing cells, circular Golgi complexes were present that were otherwise unidentified in Thr92-D2^{HY} expressing cells.

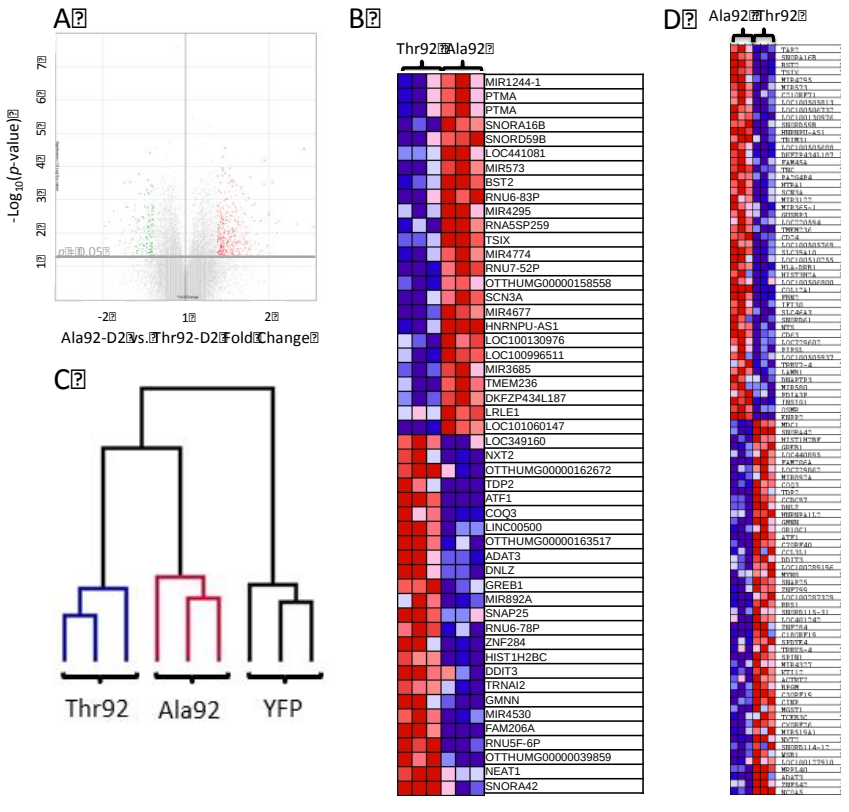

Figure 4

Figure 4. Microarray analysis of HEK-293 cells stably expressing Ala92-D2^{HY} or Thr92-D2^{HY} proteins. (A) Volcano plot of expression data in the comparison of Ala92-D2^{HY} (n = 3) with Thr92-D2^{HY} -expressing cells (n = 3); highlighted genes are significant at a *p*-value < 0.05 and a fold change > 1.3 (red) or < -1.3 (green); (B) cultured cells differing only in their stable expression of Ala92-D2^{HY} versus Thr92-D2 ^{HY} have unique transcriptional features where heat mapping of the 25 most enriched and 25 most downregulated genes as identified by fold change calculated in differential expression analysis are shown; (C) dendogram created via hierarchical clustering analysis reveals that mRNA expression patterns of Thr92-D2, Ala92-D2 and YFP-expressing cells cluster with samples of the same phenotype; Ala92-D2 cells exhibit a transcriptional expression pattern more similar to Thr92-D2-expressing cells than to YFP controls; (D) heat map of the top 50 genes up- and down-regulated genes as ranked by gene set enrichment analysis software.

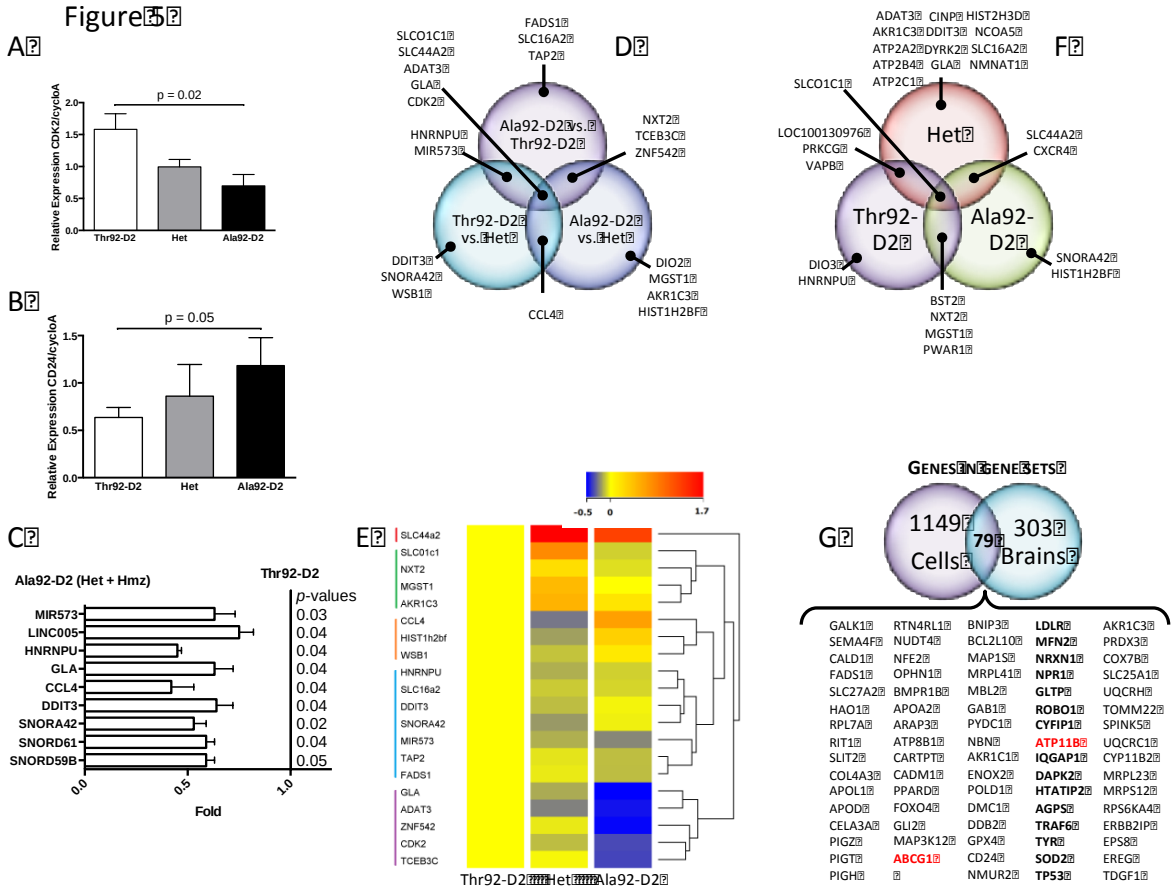

Figure 5. Identification of genes differentially affected by Ala92-D2 expression in both cells and human brains. 40 genes identified in the cell microarray (i) for their significant alteration in expression and (ii) representation of unique physiologic themes were chosen for additional studies in human brain. (A) Relative expression of CDK2 by RT-qPCR in human brain samples from Ala92-D2 and Thr92-D2 homozygotes and heterozygous; (one-way ANOVA $p = 0.01$, two-tailed t test Ala92-D2 vs. Thr92-D2, $p = 0.02$); (B) same as **A** except that CD24 was studied; (one-tailed t test Ala92-D2 vs. Thr92-D2, $p = 0.05$); (C) when expression data from heterozygous and homozygous samples were combined, significant differences in comparison to Thr92-D2 brain samples was observed for 9 genes; (D) 21 genes exhibited an expression level that varied >1.5-fold between any two genotypes; these 21 genes are depicted in a Venn diagram to show genes identified in one or more pairwise genotype comparisons; (E) hierarchical clustering of these genes (aside from DIO2) after normalization to the expression level of Thr92-D2 homozygotes using Euclidean distance metric yields a dendogram showing 5 clusters; expression levels are indicated by heatmap (low: blue; high: red) created in Agilent Genespring GX 12.6; (F) D2 expression in human brain correlated significantly (Pearson correlation at $p<0.05$) with the expression of 27 genes; Venn diagram showing overlap between genes that correlated with D2 in Thr92-D2 homozygotes, Hets and Ala92-D2 homozygotes samples; (G) 79 individual genes common to both the cell and human brain microarray gene set enrichment analyses were identified using Venn diagrams, constituting the Ala92-D2 fingerprint; these include two Golgi-specific genes (red) and 15 Golgi-related genes (bold).

Figure 6

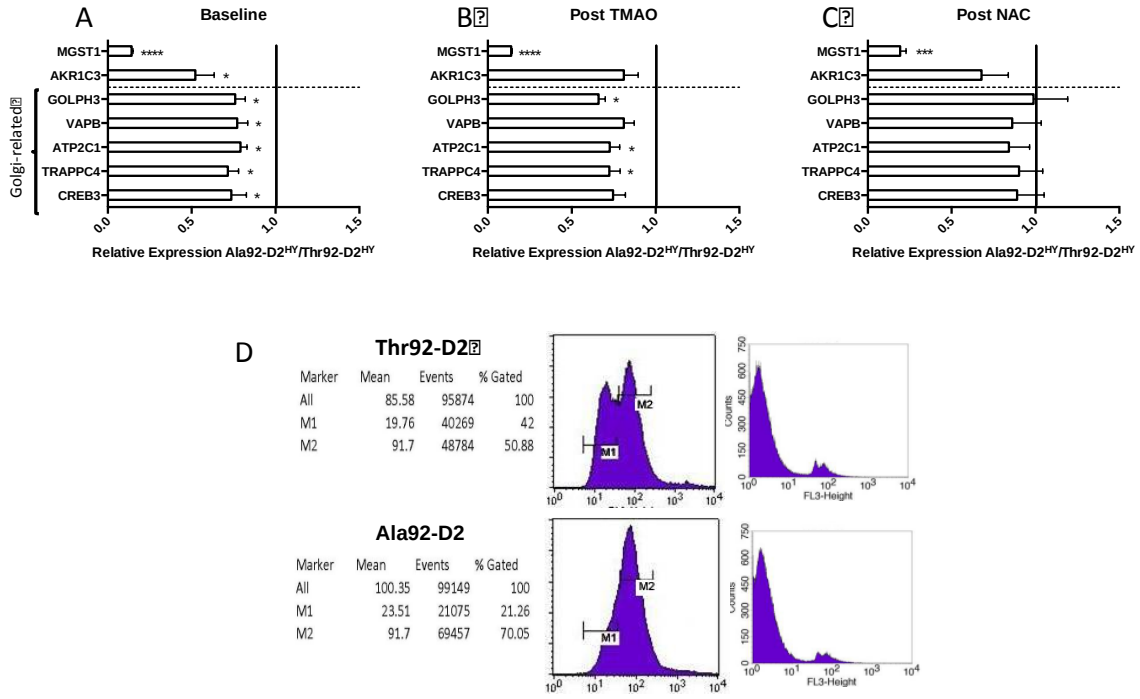

784

785 **Figure 6. Normalization of gene expression profile in Ala92-D2 expressing-cells by antioxidant and**
786 **the chemical chaperone NAC**. (A) Expression levels of genes identified in cell microarray were con-
787 firmed by RT-qPCR in Thr92-D2^{HY}- and Ala92-D2^{HY}-expressing cells where selected genes exhibited
788 lower expression levels in Ala92-D2^{HY}; (B) Treatment with chemical chaperone, trimethylamine oxide
789 (TMAO), normalizes two genes; (B) After 24 h of treatment with N-acetylcysteine (NAC), the expression
790 levels of the Golgi-related genes normalized with respect to their expression levels in Thr92-D2^{HY}-ex-
791 pressing cells; (two-tailed t tests *p≤0.05, *** p≤0.001, ****p≤0.0001, all data are the mean ± SEM of 3
792 entries per data-point); (D) The early stage of apoptosis was examined by annexin V/propidium iodide
793 staining of intact cells; cells were gated per YFP signal, annexin V-PE/propidium iodide were FL2/FL3.
794 Left two panels are annexin V-PE staining where M1 represents non-apoptotic cells and M2 represents

apoptotic cells; right two panels are propidium iodide staining to differentiate late-apoptotic from necrotic cells.

Supplementary Figure Legends

Supplemental Figure 1

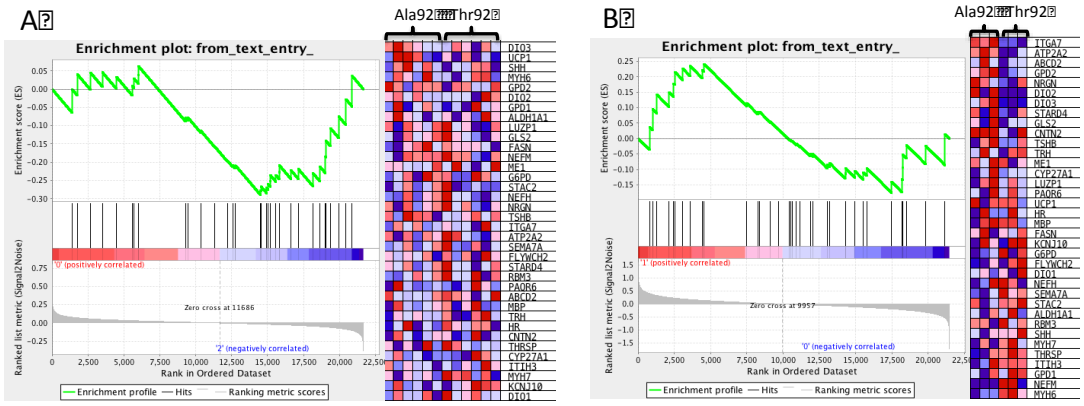

Figure S1. Ala92-D2 homozygous brain samples and Ala92-D2HY-expressing cells do not exhibit transcriptional evidence of hypothyroidism. (A) The complete microarray dataset for all 12 Ala92-D2 and Thr92-D2 homozygous brain samples was analyzed by gene set enrichment analysis (GSEA) using a custom gene set of known T3-responsive genes (18, 19) (Table S4). Enrichment plot and heat map, both generated in GSEA (Broad Institute), demonstrate enrichment patterns for this custom gene set where the gene set was not found to be enriched (nominal *p*-value 0.835, FDR 0.842); (B) Also, this T3-responsive

custom gene set was not enriched in the Ala92-D2 vs. Thr92-D2 cell microarray (nominal *p*-value 0.604, FDR 0.701).

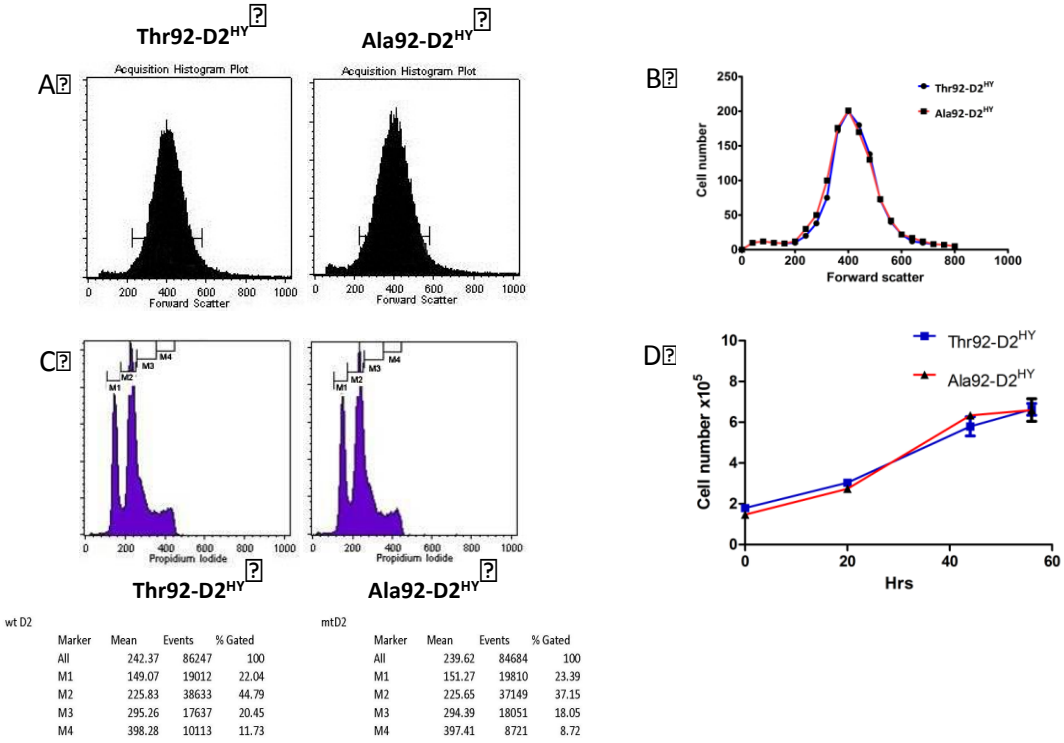

Supplemental Fig. 2

Figure S2. HEK-293 cells stably expressing Ala92-D2^{HY} exhibit normal growth and division (A) Cell size was analyzed by distribution of forward scatter signal from FACS instrument; (B) Two forward scatter distribution curves from Thr92-D2^{HY} and Ala92-D2^{HY} were superimposed for comparison; (C) Cell cycle was analyzed by propidium iodide staining after fixation. M1, M2, M3, M4 region denotes subG1, G0/G1, S, G2/M stages of cell cycle respectively; (D) Cell growth was analyzed by counting cells after plating.

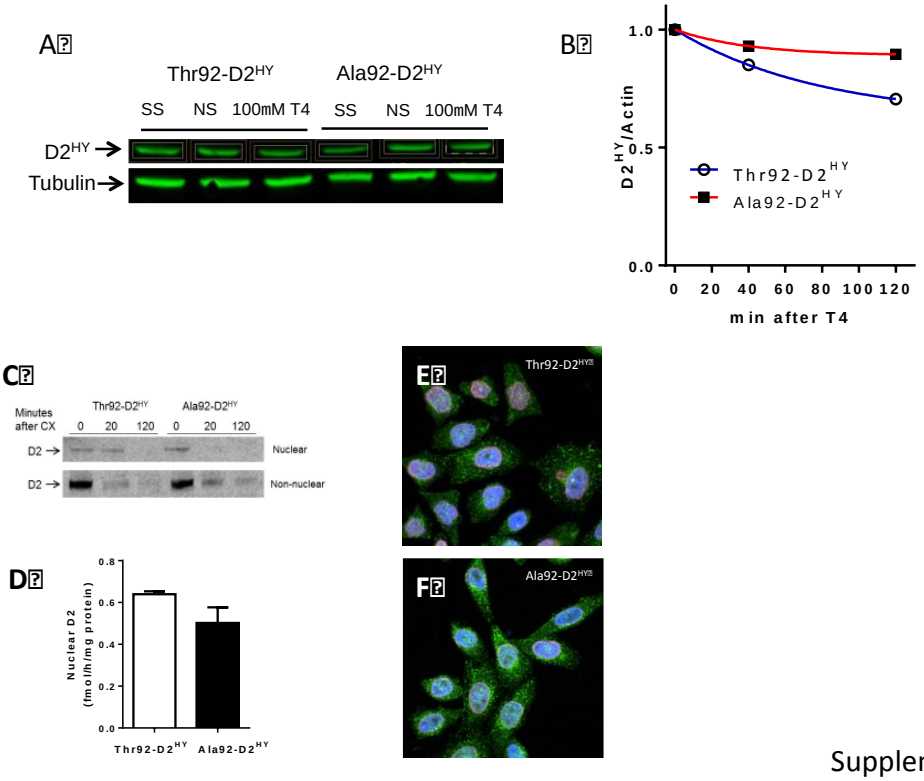

Supplemental Fig. 3

Figure S3. Ala92-D2^{HY} lingers after exposure to T4. (A) Thr92-D2^{HY} and Ala92-D2^{HY} cells were incubated for 120 min with three different conditions, stripped serum (SS, which has no T4), normal fetal bovine serum (NS) and 100 □M T4 with fetal bovine serum and subsequently harvested and processed for western analysis using □YFP and □Tubulin. Whereas Thr92-D2^{HY} decreases in response to T4, its natural substrate, Ala92-D2^{HY} levels decrease only slightly suggesting impaired degradation via ubiquitination; (B) Thr92-D2^{HY} and Ala92-D2^{HY} cells were incubated for 120 min with 100 uM T4 and subsequently harvested and processed for western analysis using □YFP and □Tubulin; data from 3 independent experiments were pooled; (C) the indicated cells were incubated for 20-120 min with 100 uM CHX and subsequently harvested and processed for western analysis of D2^{HY} proteins in cell lysates or in nuclear fractions using □YFP and □Actin; (D) D2 activity of isolated nuclear fractions after treatment with CHX; values are the mean ± SEM of 5 entries per data-point; (E-F) immunofluorescence of HEK-293

827 cells stably expressing D2^{HY} proteins; D2 was stained with YFP (green) and is found throughout the

828 ER, nuclei were stained with DAPI (blue), and overlap with nuclear lamin (red) is also visualized.

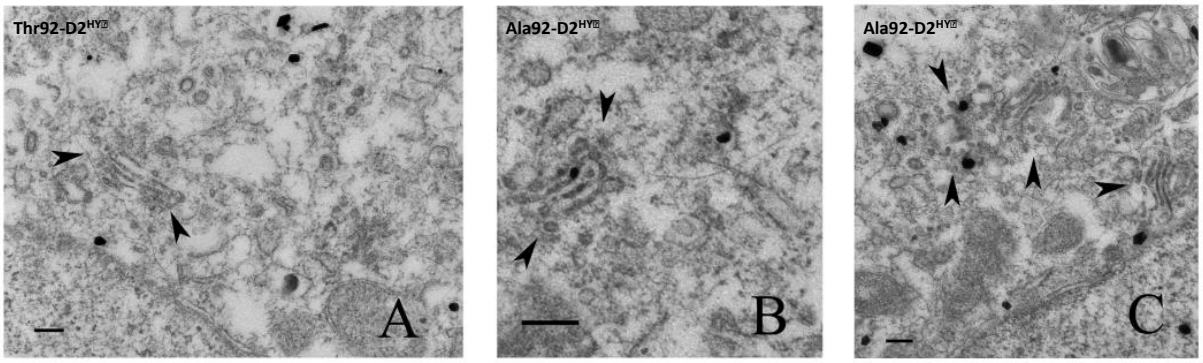

Supplemental Fig. 4

829

830 **Figure S4. Only Ala92-D2^{HY} can be found in the Golgi apparatus after treatment with cyclo-**

831 **heximide.** (A) Thr92-D2^{HY} cells treated with CHX (100 μg/ml) for 2 hours lack silver grains denoting

832 localization of D2^{HY} within the Golgi apparatus (arrows indicate Golgi); (B,C) Ala92-D2HY can be read-

833 ily visualized within the Golgi apparatus in CHX-treated cells; scale bars = 0.25 μm.

Supplemental Fig. 5

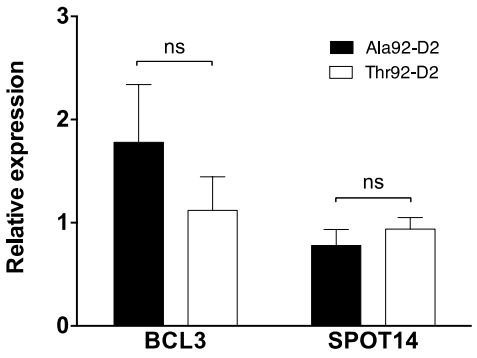

834

835 **Figure S5. Expression of T3-responsive genes in HeLa cells co-cultured with Thr92-D2^{HY} or Ala92-**
836 **D2^{HY}-expressing cells did not differ.** When HeLa cells were grown in a previously characterized co-cul-
837 ture system(33) with Thr92-D2^{HY}- (n = 6) or Ala92-D2^{HY}-expressing (n = 6) cells, no differences in the
838 expression of either T3-responsive gene were observed (BCL3: *p*-value 0.33, two-tailed t test; SPOT14:
839 *p*-value 0.42, two-tailed t test).

Supplemental Fig. 56

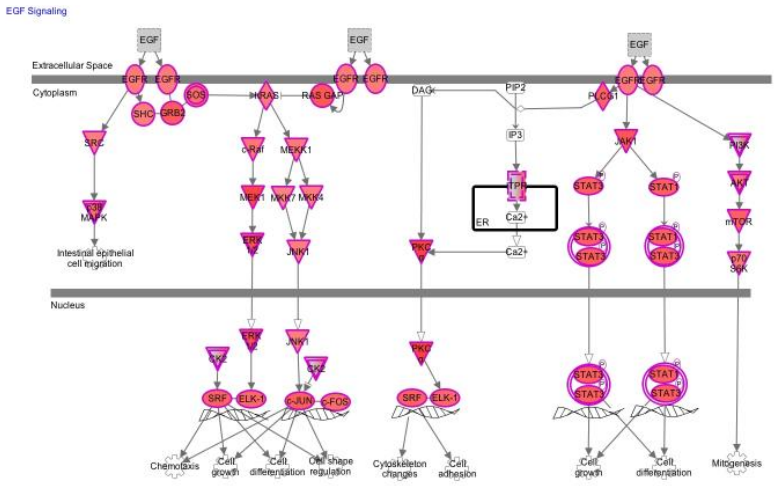

840

841 **Figure S6. 50/56 Genes within the EGF Signaling Canonical Pathway are Altered in Human Brains**.

842 When pathway analysis was performed on the complete microarray dataset from human brain samples

843 from Ala92-D2 homozygotes, Hets, and Thr92-D2 homozygotes (n = 19), the EGF Signaling pathway

844 diffuse alterations in genes within this pathway were identified (*p*-value < 0.001, ratio 50/56) from the

845 receptors themselves to downstream signaling molecules.

846

A

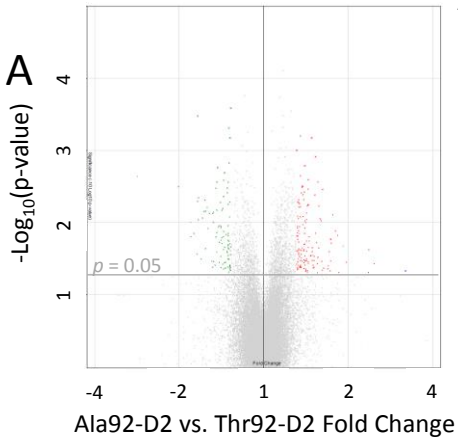

B

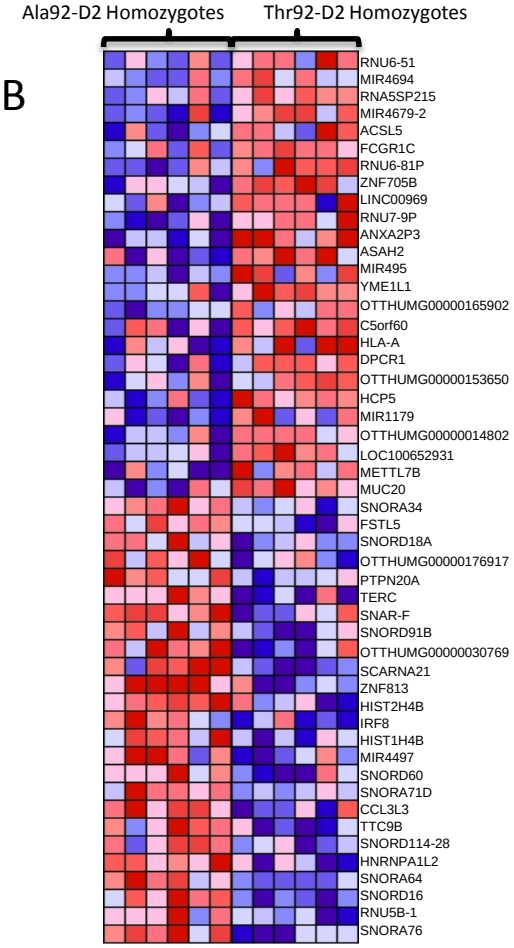

C

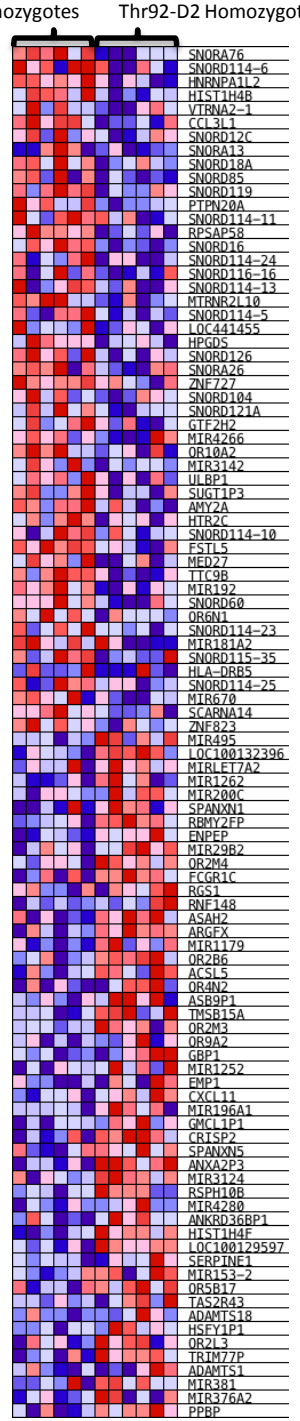

D

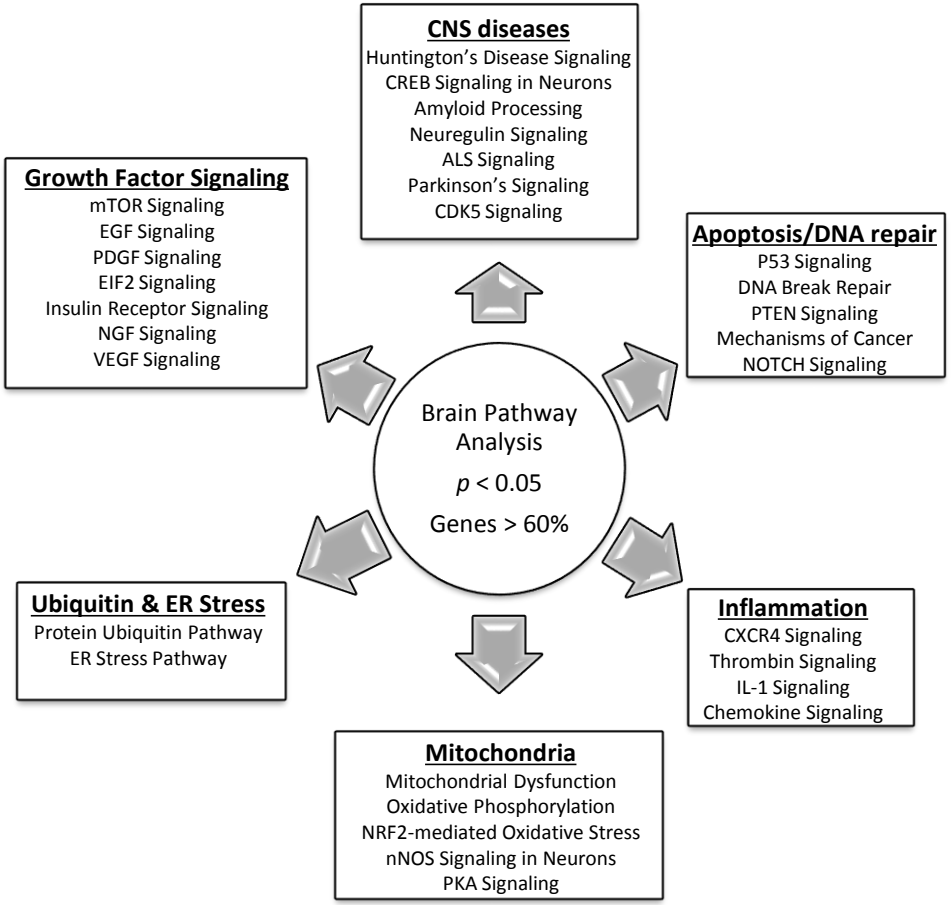

Figure 1

Figure 2

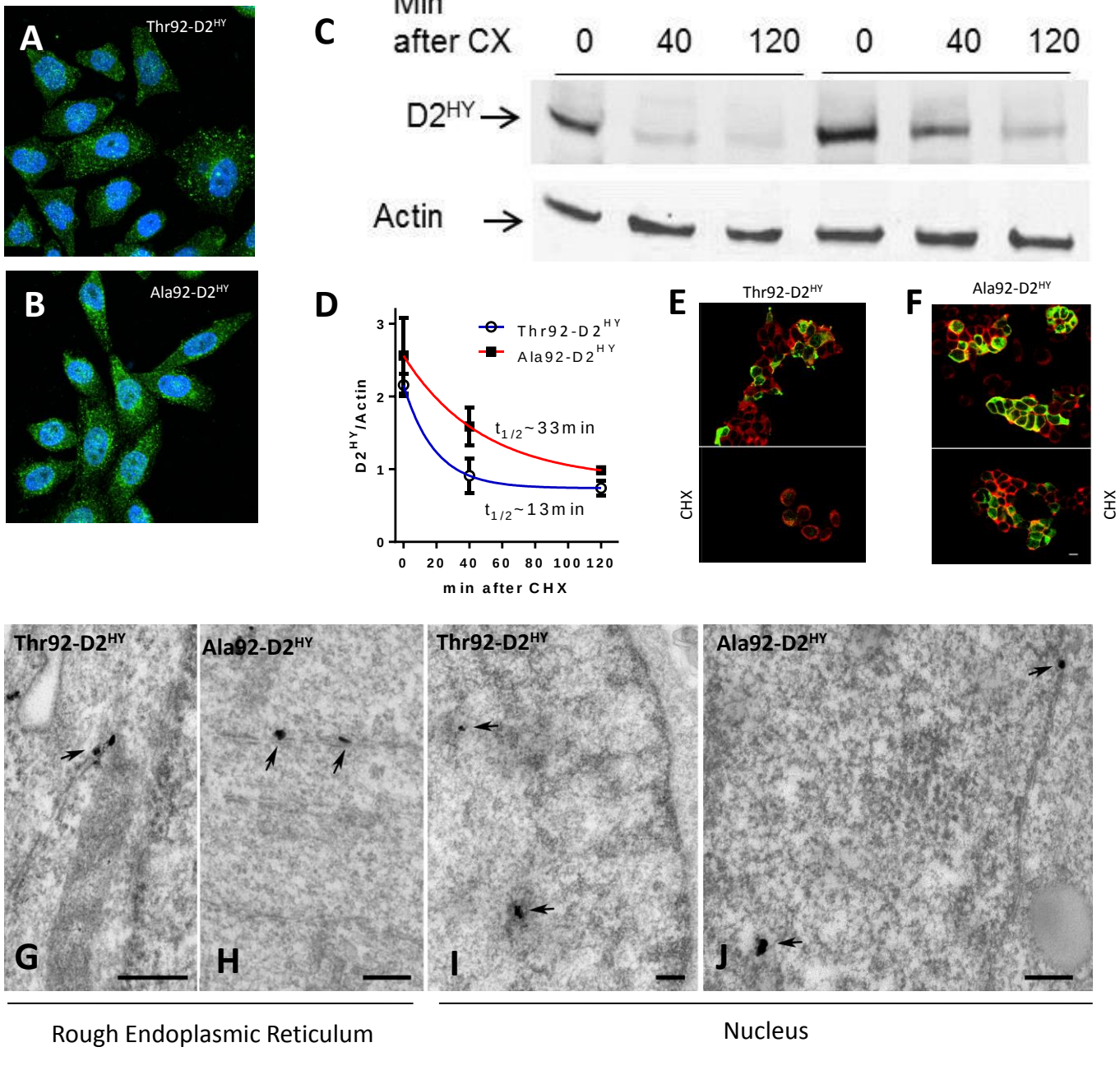
A
Thr92-D2HY
B
Ala92-D2HY
C
Thr92-D2HY
Ala92-D2HY
Min after CX
0
40
120
0
40
120
D2HY
Actin
D
Thr92-D2HY
Ala92-D2HY
D2HY/Actin
t1/2~33min
t1/2~13min
min after CHX
E
Thr92-D2HY
CHX
F
Ala92-D2HY
CHX
G
Thr92-D2HY
H
Ala92-D2HY
I
Thr92-D2HY
J
Ala92-D2HY
Rough Endoplasmic Reticulum
Nucleus

Figure 3

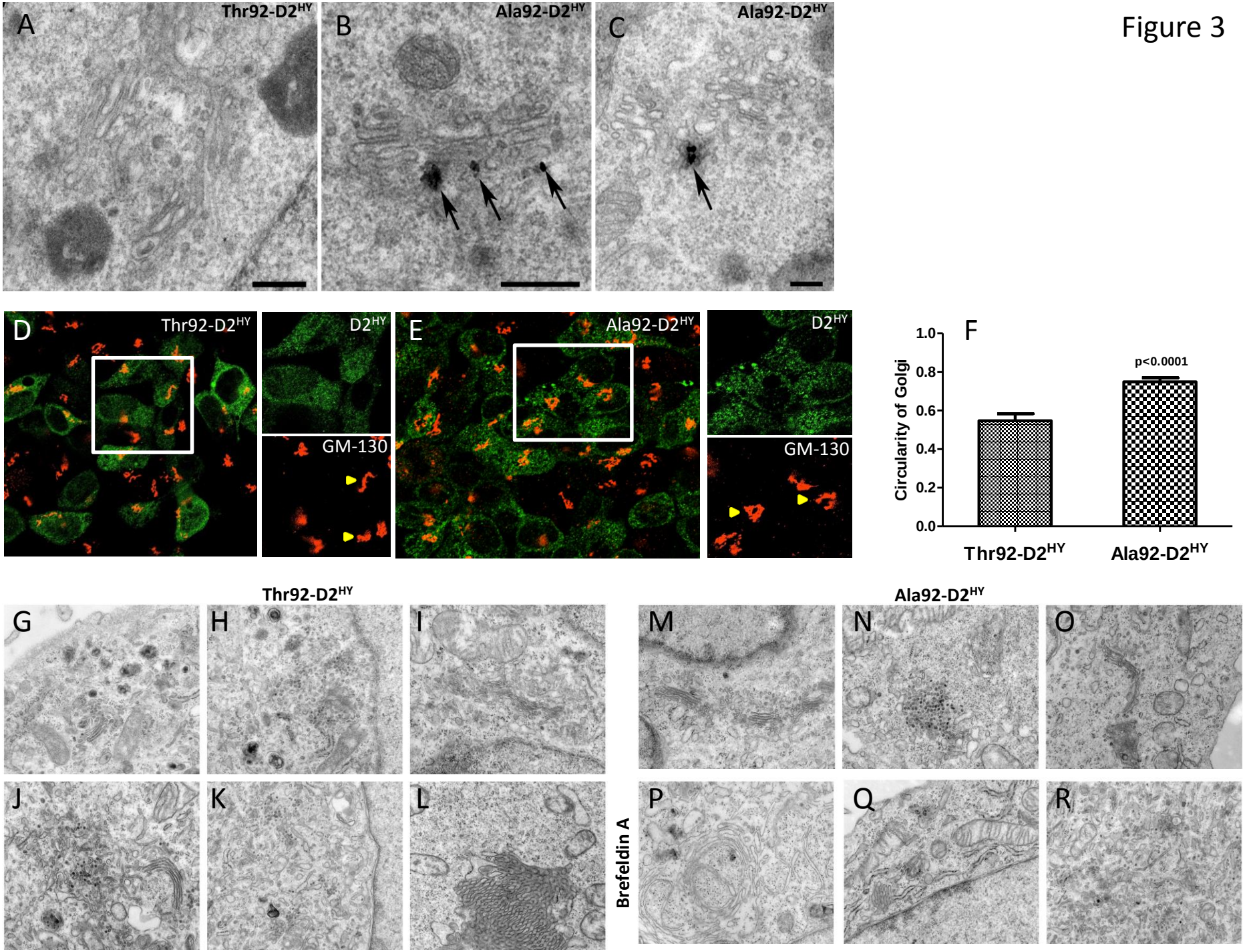
A
Thr92-D2HY
B
Ala92-D2HY
C
Ala92-D2HY
D
Thr92-D2HY
D2HY
GM-130
E
Ala92-D2HY
D2HY
GM-130
F
Circularity of Golgi
1.0
0.8
0.6
0.4
0.2
0.0
p<0.0001
Thr92-D2HY
Ala92-D2HY
Thr92-D2HY
Ala92-D2HY
G
H
I
M
N
O
Brefeldin A
J
K
L
Brefeldin A
P
Q
R

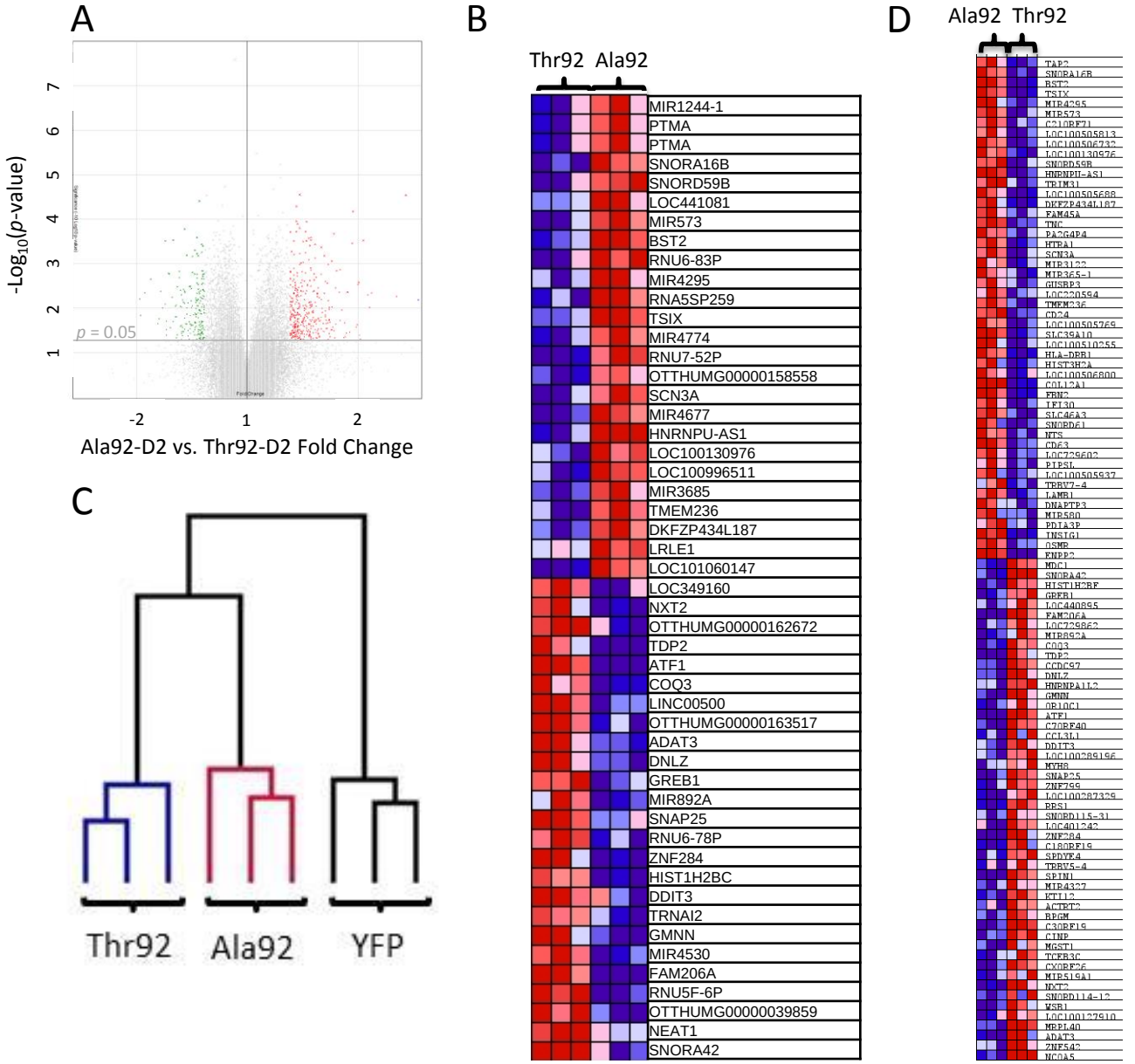
A
-Log10(p-value)
p = 0.05
Ala92-D2 vs. Thr92-D2 Fold Change
B
Thr92 Ala92
MIR1244-1
PTMA
PTMA
SNORA16B
SNORD59B
LOC441081
MIR573
BST2
RNU6-83P
MIR4295
RNA5SP259
TSIX
MIR4774
RNU7-52P
OTTHUMG00000158558
SCN3A
MIR4677
HNRNPU-AS1
LOC100130976
LOC100996511
MIR3685
TMEM236
DKFZP434L187
LRLE1
LOC101060147
LOC349160
NXT2
OTTHUMG00000162672
TDP2
ATF1
COQ3
LINC00500
OTTHUMG00000163517
ADAT3
DNLZ
GREB1
MIR892A
SNAP25
RNU6-78P
ZNF284
HIST1H2BC
DDIT3
TRNAI2
GMNN
MIR4530
FAM206A
RNU5F-6P
OTTHUMG00000039859
NEAT1
SNORA42
C
Thr92
Ala92
YFP
D
Ala92 Thr92

Figure 4

Figure 5

A

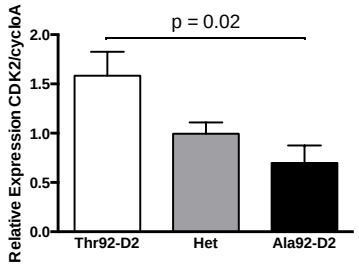

B

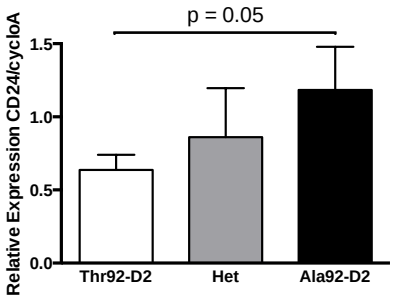

C

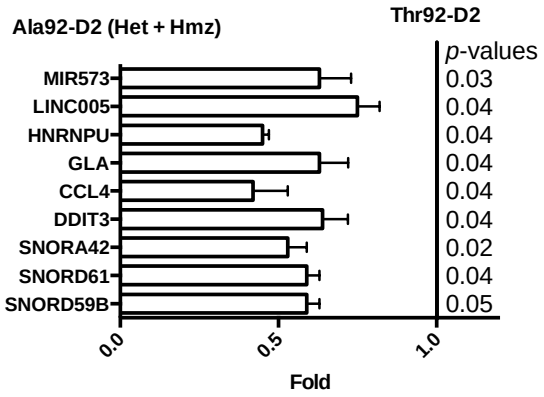

D

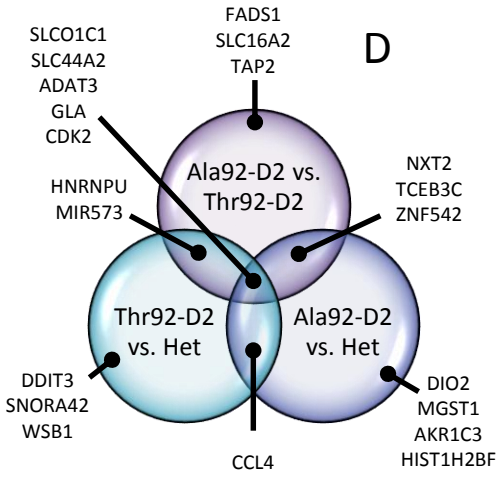

E

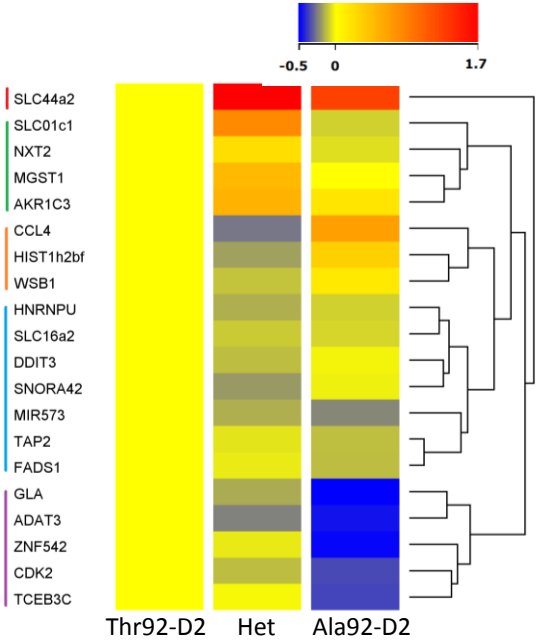

F

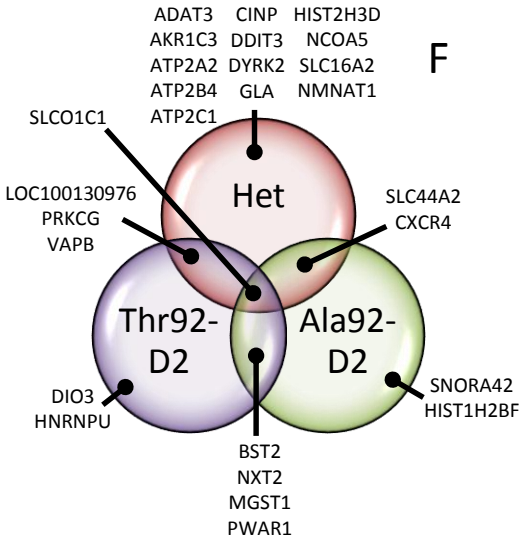

G

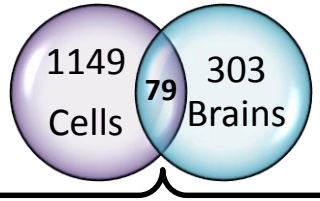

GALK1	RTN4RL1	BNIP3	**LDLR**	AKR1C3
SEMA4F	NUDT4	BCL2L10	**MFN2**	PRDX3
CALD1	NFE2	MAP1S	**NRXN1**	COX7B
FADS1	OPHN1	MRPL41	**NPR1**	SLC25A1
SLC27A2	BMPR1B	MBL2	**GLTP**	UQCRH
HAO1	APOA2	GAB1	**ROBO1**	TOMM22
RPL7A	ARAP3	PYDC1	**CYFIP1**	SPINK5
RIT1	ATP8B1	NBN	**ATP11B**	UQCRC1
SLIT2	CARTPT	AKR1C1	**IQGAP1**	CYP11B2
COL4A3	CADM1	ENOX2	**DAPK2**	MRPL23
APOL1	PPARD	POLD1	**HTATIP2**	MRPS12
APOD	FOXO4	DMC1	**AGPS**	RPS6KA4
CELA3A	GLI2	DDB2	**TRAF6**	ERBB2IP
PIGZ	MAP3K12	GPX4	**TYR**	EPS8
PIGT	**ABCG1**	CD24	**SOD2**	EREG
PIGH		NMUR2	**TP53**	TDGF1

Figure 6

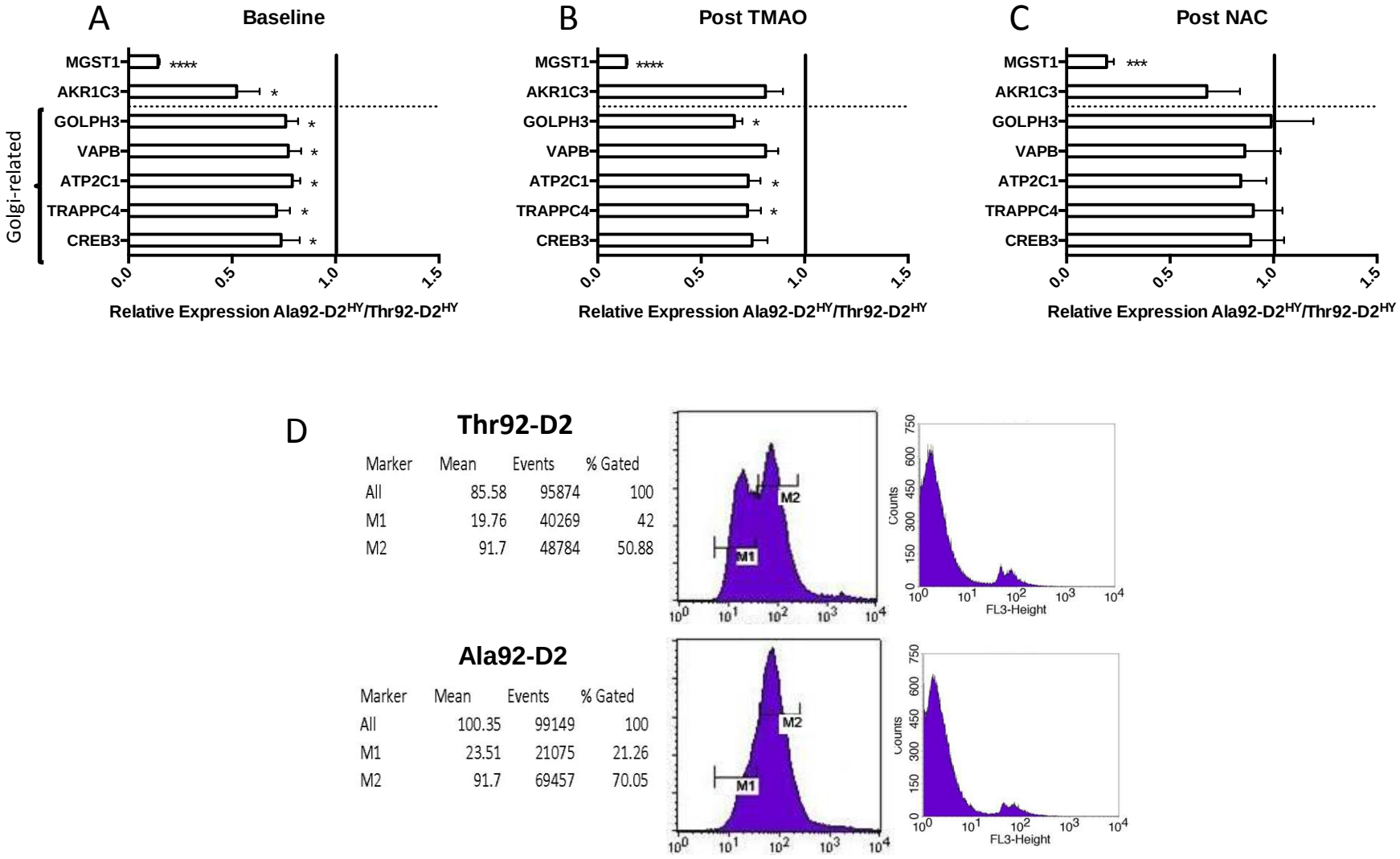
A
Baseline
B
Post TMAO
C
Post NAC
MGST1
AKR1C3
GOLPH3
VAPB
ATP2C1
TRAPPC4
CREB3
Golgi-related
****
***
*
0.0
0.5
1.0
1.5
Relative Expression Ala92-D2HY/Thr92-D2HY
D
Thr92-D2
Marker Mean Events % Gated
All 85.58 95874 100
M1 19.76 40269 42
M2 91.7 48784 50.88
Ala92-D2
Marker Mean Events % Gated
All 100.35 99149 100
M1 23.51 21075 21.26
M2 91.7 69457 70.05
M1
M2
Counts
FL3-Height